Aerospace Science and Technology 138 (2023) 108349

Contents lists available at ScienceDirect

Aerospace Science and Technology

journal homepage: www.elsevier.com/locate/aescte

Robust multidisciplinary analysis and optimization for conceptual design of flexible aircraft under dynamic aeroelastic constraints

Marco Saporito [a,b], Andrea Da Ronch [a,*], Nathalie Bartoli [b], Sébastien Defoort [b]

[a] University of Southampton, University Rd, Southampton, SO171BJ, UK
[b] ONERA/DTIS, Université de Toulouse, 2 Av. Edouard Belin, Toulouse, F–31055, France

ARTICLE INFO

Article history:
Received 9 December 2022
Received in revised form 27 March 2023
Accepted 14 April 2023
Available online 20 April 2023
Communicated by Mehdi Ghoreyshi

Keywords:
Overall aircraft design
Aeroelasticity
MDAO
Conceptual design
Flutter
Gust loads

ABSTRACT

We present a computational framework for robust multidisciplinary design and optimization of flexible aircraft, suited for the conceptual design exploration phase. Constraints are representative of some dynamic aeroelastic effects, including flutter and gust-induced structural stresses. Uncertainties on wing structural parameters are considered, and reliability-based optimization under dynamic aeroelastic constraints is addressed by a Bayesian approach. This work details the implementation aspects, covering disciplinary software tools and the overall aircraft design suite, the optimization algorithm and the approach to propagate uncertainty efficiently. Results are thoroughly discussed for a reference aircraft, which is optimized in the study with respect to a few wing parameters including aspect ratio. The proposed approach is compared to a conventional design methodology assuming a rigid airframe. We show that when applied to slender and flexible wings, the latter can produce dangerous non-conservative results, as its predictions are too optimistic both with respect to efficiency and to aeroelastic safety.

1. Introduction

As environmental requirements become more and more stringent, reduction of emissions in commercial aviation is targeted with increasing pressure both by research and industry [1,2]. A large effort is addressed at the exploration of disruptive technologies and configurations that may lead to a new generation of highly efficient aircraft. From the aerodynamic side, one interesting innovation axis is towards high aspect ratio, flexible configurations, such as slender truss-braced wings [3,4] or semi-aeroelastic hinged wing tips [5].

Due to the multi-faceted characteristics of airplane design, the implementation of such disruptive solutions demands the ability to deal with technical disciplines that are increasingly interconnected. High aspect ratio wings exacerbate fluid-structural interaction issues, such as flutter and gust loads, and affect stability, control strategies and pilot coupling [6]. Hence, an effective exploration of disruptive concepts needs to be accompanied by analysis and optimization frameworks that are as multidisciplinary as possible, starting from the conceptual stage [7]. For this reason, a new paradigm of physics-based and integrated aircraft conceptual design is being introduced to replace the classical approach of knowledge-based sectorial design [8–10]. When dealing with flexible airframes, as is the case in this work, a challenging aspect is aeroelasticity. On the one hand, there are important safety implications: large structural deformations, flutter and the response to gusts are potentially dangerous phenomena that need to be cautiously analyzed. On the other hand, they require significant computational capabilities, both in terms of model complexity and computational time. Therefore, including an assessment on these aspects during the conceptual design of high aspect ratio aircraft remains an active research challenge, involving different concurrent domains and a large body of literature [11–14]. It is clear that in this kind of complex and expensive multidisciplinary analysis and optimization (MDAO) studies, the efficiency of the optimization algorithm and the robustness of the disciplinary analysis tools are key to the success of the approach. Not surprisingly, a great research effort was spent over the years in the development of efficient MDO architectures and optimization algorithms [15–17]. A promising optimization approach, which this work pursues, is the Super-Efficient Global Optimization (SEGO), a Bayesian Optimization technique originally proposed by [18], currently the topic of several research programs proposing continuous improvements [19–21].

The complexity of MDAO applied to novel concepts increases by the inherent lack of knowledge the designer has of those new and unseen concepts that radically depart from the common tube-and-wing configuration. This, combined with the need for large

* Corresponding author.
E-mail address: a.da-ronch@soton.ac.uk (A. Da Ronch).

https://doi.org/10.1016/j.ast.2023.108349

and fast design exploration, imposes the use of low- or medium-fidelity tools, introducing underlying approximations that result in possible risks due to uncalibrated predictions. For these reasons, uncertainty quantification and management in MDAO applications have become interesting challenges, currently the centre of several research activities [22]. If properly addressed, it would improve the quality of the design outcomes providing key information on the robustness and reliability of the results. Despite most studies on aircraft conceptual design and optimization rely on deterministic processes, assuming the feasibility of their results and ignoring the concept of robustness, some studies do face the issue of uncertainty quantification and propagation, although not necessarily including aeroelasticity-related issues. Pioneering work on this topic was done by [23], whereas recent publications including uncertainty on flying qualities or aeroelastic performances can be found, for example, in [24,25].

Given the above context, this work proposes a framework for robust MDAO for the conceptual design of flexible transport aircraft. The presented architecture is not only capable of taking into account static and dynamic aeroelasticity, but also to perform uncertainty propagation of some key input parameters into a series of aeroelastic constraints, providing the designer with an assessment on the reliability of the optimal design solution.

The work continues in Section 2 with an overview of the proposed case study and framework architecture. Then, a more detailed description of the disciplinary methods and tools is provided in Section 3, covering in particular the aeroelastic models, the overall aircraft design tool, the optimization strategy and the uncertainty quantification approach. Section 4 describes the sizing process for the flexible wing, including quantitative example applications. Section 5 is related to the dynamic aeroelastic constraints on flutter and gust loads. It also includes sensitivity analysis results that will help the setup of the overall robust MDAO problem. The optimization results for the proposed case study are provided and discussed in Section 6. Then, some additional parametric studies are presented in Section 7 to gain further insights about the effects of aspect ratio variations and of the probabilistic aeroelastic constraints. Finally, conclusions and perspectives are drawn in Section 8.

2. Problem overview

The objective of the proposed case study is to optimize the fuel burn of an A320-like, flexible configuration for a representative flight, with respect to some wing planform parameters, including the aspect ratio. To this end, some tools were developed and interfaced to extend the design capabilities of an existing, conventional aircraft design tool, in order to take into account the main aeroelastic problems of high aspect ratio wings, and the effect of uncertainties in the wing structural model. More in detail, the optimization is performed ensuring that:

- The wing is considered flexible and its structure is properly sized using static aeroelastic loads;
- The weight of the sized wing is optimal with respect to an identified set of structural parameters;
- The overall aircraft design process takes into account the eventual corrections on wing weight due to the aeroelastic sizing;
- The wing does not undergo plastic deformation or structural failure under gust loads, computed on the flexible wing;
- The wing is flutter-free within the prescribed flight envelope;
- Compliance with gust loads and aeroelastic flutter requirements can be granted not only in a deterministic way, but also in a robust way, propagating some key structural model uncertainties.

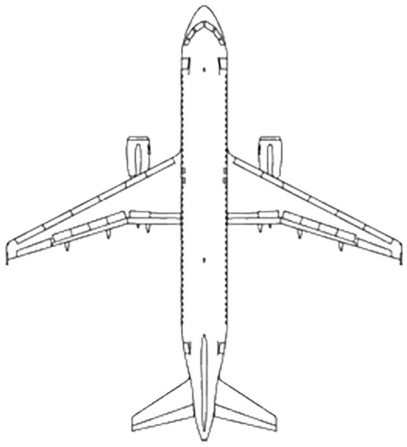

Fig. 1. CeRAS baseline planform, from [26].

Table 1
CeRAS baseline parameters, from [26].

Top Level Aircraft Requirements	
Number of passengers	150
Passenger weight [lbs]	200
Design Range [NM]	2750
Operational Range [NM]	800
Cruise Mach number	0.78
Approach speed [kts]	132
Planform parameters	
Wing area [m^2]	122.4
Mean aerodynamic chord (MAC) [m]	4.2
Aspect ratio	9.48
Wing break	0.40
Wing sweep (25% chord) [deg]	24.5
Wing taper ratio	0.313
Horizontal tail sweep (25% chord) [deg]	28.0
Horizontal tail taper ratio	0.300
Propulsion	
Max thrust at sea level [N]	117880

The reference configuration is the CeRAS baseline, shown in Fig. 1. The main characteristics are summarized in Table 1. The proposed MDAO architecture is outlined in Fig. 2. The overall optimization process involves the input variables V_g, which refer to a desired set of aircraft geometry parameters. The Multi-Disciplinary Analysis (MDA) is handled by an aeroelastic sizing routine, ensuring the overall aircraft sizing process is consistent with the aeroelastic sizing of the wing. It is important to note that the flexible wing sizing is performed by use of a developed aeroelastic module (see Section 3.1), while the overall aircraft sizing is run by a different, dedicated tool (`FAST-OAD`, described in Section 3.2). The latter does not take into account any effect of structural flexibility, nor does it build any structural model to predict the stresses. It only adopts traditional rigid-body equations and semi-empirical regressions based on existing conventional aircraft to estimate performance and weight and balance characteristics. The tool allows for some technological correction factors taking into account some optional features or components. An exemplary correction factor would account for the drag build-up due to the installation of winglets. Herein, the technological correction factor, k_w, is employed to correct the estimation of the flexible wing structural weight. This is done as explained in the following paragraphs.

The first step is to launch `FAST-OAD` with no correction applied, $k_w = 1$, based on the input geometric variables V_g and some Top Level Aircraft Requirements (TLARs) such as aircraft range, passenger number, approach speed, etc., as shown in Table 1. The sizing process provides a sized rigid aircraft, which satisfies the

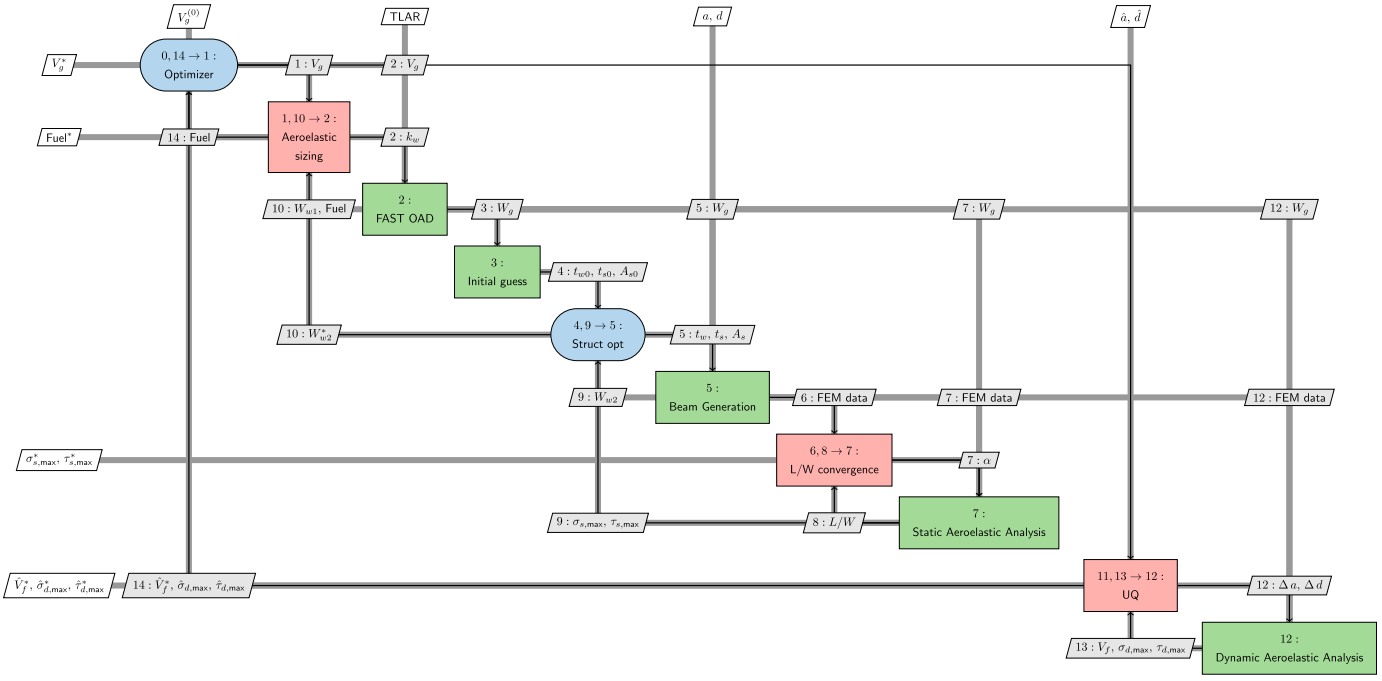

Fig. 2. Extended design structure matrix (XDSM) of the present robust MDAO framework for aeroelastic sizing and fuel burn optimization of a transport aircraft. The XDSM convention follows [15].

TLARs, with a certain amount of fuel burn required, and a wing structure of weight W_{w1}. This value is collected and stored by the aeroelastic sizing routine. It is worth pointing out here that the fuel burn, which is used as objective for the overall optimization, is the one calculated for the rigid aircraft. It is assumed here that structural deformation adds a negligible effect to the overall aircraft drag polar, so no effort is made to apply such a correction. The aspect ratio effect on drag is kept equal to one for a rigid configuration. The reason to include the aeroelastic analysis is to capture the effects on structural integrity, which have a strong impact on weight and safety. Based on the sized rigid body wing geometry, completely identified by the parameters W_g, an approximated wing-box structural model is initialized. The wing-box model is characterised by the web thickness, t_w, skin thickness, t_s and stringers cross section area, A_s. At first, the wing-box model is initialized using a simple analytical approach assuming a rigid airframe, which provides the initial guess t_{w0}, t_{s0}, A_{s0}. Then, a structural optimization is performed in a neighbourhood of $[t_{w0}, t_{s0}, A_{s0}]$ to minimize the wing structural weight W_{w2} with the constraints that the static normal and shear stresses of the structure, $\sigma_{s,\max}$ and $\tau_{s,\max}$, respectively, do not exceed the material - aluminium - yield strength. This time, loads are computed on the elastic wing, requiring an aeroelastic model to be generated. This is done through a beam generation module that computes the needed elastic properties from the wing box geometry and condensates them into an equivalent finite element beam model. The beam properties (`FEM data`) are passed to the aeroelastic solver, which couples the nonlinear beam solver with the Vortex Lattice Method (VLM) aerodynamics to compute the structural loads on the elastic wing. This analysis is run at a prescribed load factor, $n = L/W$. As the structural nonlinearity introduces a nonlinearity in the lift slope of the wing, the angle of attack providing the required load factor cannot be determined directly, and has to be calculated iteratively. Once the load factor is matched, the structural stresses are stored and used to constrain the structural optimization process. After the latter has converged to the best structural weight W_{w2}^*, this value is compared with the wing structural weight W_{w1} estimated by `FAST-OAD`. If $W_{w1} \approx W_{w2}^*$, then the design is consistent and the sizing process is terminated. If $W_{w1} \neq W_{w2}^*$, a correction factor k_w is generated to make `FAST-OAD` size a new airplane with a different wing weight. Generally, this produces a different configuration W_g with a different wing-box and a different aeroelastic behaviour. The aeroelastic sizing and optimization on the new wing is repeated until a new W_{w2}^* is computed. The process is iterated until a consistent design is found with $W_{w1} \approx W_{w2}^*$. Once a consistent design is achieved, the dynamic aeroelastic behaviour of the candidate is investigated next. At this point, the dynamic aeroelastic solvers are called to evaluate either the flutter boundary or the gust loads, or both. The outputs (the flutter speed V_f, or the maximum dynamic axial and shear stresses $\sigma_{d,\max}$ and $\tau_{d,\max}$) can be used as constraints for the overall MDAO.

In this work, the dynamic aeroelastic constraints are implemented in the form of reliability constraints. Constraints are formulated in a probabilistic manner to insure robustness against the user-specified input uncertainty. The input uncertainty can be attributed, for example, to the elastic axis (EA) location, a, and its distance d from the centre of gravity (CG) axis of the wing. Prescribed distributions $\hat{a}$ and $\hat{d}$ are given to the uncertainty quantification module that propagates the uncertainty into the needed quantities of interest, producing the output distributions $\hat{V}_f$, $\hat{\sigma}_{d,\max}$ and $\hat{\tau}_{d,\max}$. At this point, the constraints are translated into probabilistic inequalities, requiring that the probability of failure is lower than a prescribed acceptable probability threshold.

The process described this far is repeated for each design candidate corresponding to different values of the V_g vector. The best candidate, minimizing fuel burn while satisfying the aeroelastic reliability constraints, is searched for using a Bayesian optimization algorithm, as it will be discussed later.

3. Analysis tools

The main tools and methods adopted in this study are here presented. The disciplines relevant to the aeroelastic module are discussed in Section 3.1, while Section 3.2 presents the overall aircraft design tool `FAST-OAD`. Section 3.3 describes the adopted

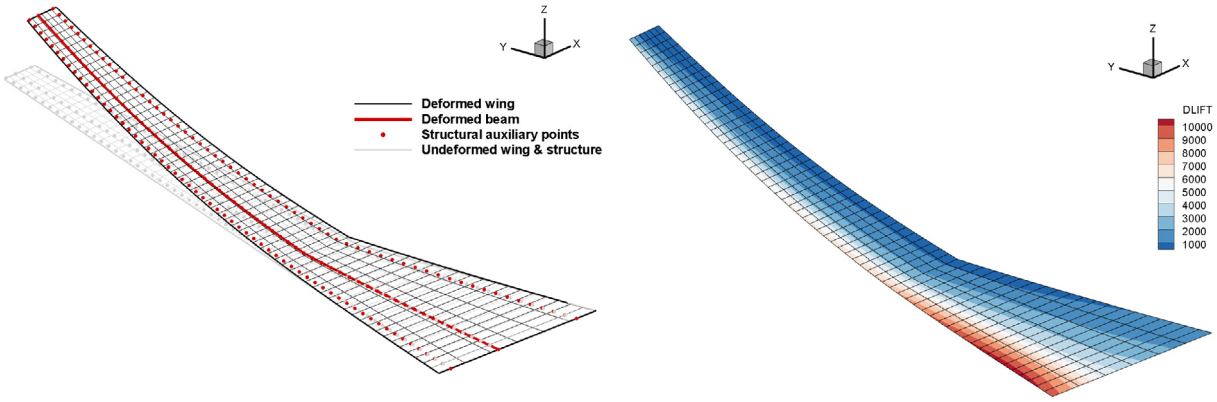

(a) Details of the aerodynamic and structural discretizations

(b) Contour plot for the lift distribution

Fig. 3. 3D views of the aeroelastic model employed, showing both the VLM discretization and the beam model, including the auxiliary structural points needed for the fluid-structure interpolation. (For interpretation of the colours in the figure(s), the reader is referred to the web version of this article.)

optimization approach based on the `SEGOMOE` suite. Finally, Section 3.4 illustrates the uncertainty quantification methodology and the `Uncertainpy` tool.

3.1. Aeroelasticity

A linear and a nonlinear aeroelastic approach are offered within the present framework. The choice of which aeroelastic approach to use depends on the specific needs of the testcase. Their main features are briefly illustrated next.

A common approach to model the aerodynamic loads for aeroelastic applications is to treat each wing section through unsteady 2-dimensional potential aerodynamics [27,28]. In this way any cross-flow and viscous effects are neglected. The computational burden remains therefore limited and suitable for early design exploratory evaluations. The potential flow assumption is valid for linear aerodynamic regimes, i.e. moderate angles of attack and subsonic speed [29]. Within this range, even the unsteady effects can be included keeping a linear formulation. A linear unsteady aerodynamic model becomes a useful tool for treating aeroelastic systems flying in relatively benign conditions (small angles of attack, small gust amplitude or control deflections, negligible cross-flow or sideslip), because it allows the full aero-structural system to be described linearly, and this, in turn, allows standard eigenvalue analysis or control studies to be performed [30,31]. Therefore, the method enables, for instance, fast predictions of flutter/divergence speed, including open-loop and closed-loop cases. Despite the above limitations, it is generally accepted for aeroelastic computations at conceptual design, especially if applied to high aspect ratio wings. As stated in [12], although it fails to capture the 3D wing tip effects, strip theory remains an accepted method for the aerodynamic response of high aspect ratio wings [32,33], thoroughly validated in the literature [34,35].

In the linear model, the aerodynamic loads are derived from the 2D unsteady potential theory of Theodorsen [36], and considered continuously distributed along the wingspan. The arbitrary motion of the aerofoil can be evaluated by means of convolution of Wagner's function. The aeroelastic model was completed by coupling the aerodynamic solver with a linear beam model representing the wing structure. A detailed description of this formulation and its numerical implementation can be found in [30]. This model is integrated in the present framework in order to perform linear flutter analysis

Despite linear models are widely accepted for flutter analysis, the effects of large deformations remain important, especially for static wing sizing [37], and therefore it is desirable to have the capability to capture them. For this reason, this framework includes a nonlinear structural solver interfaced with steady and unsteady VLM modules. Again, the wing structure is represented by a beam model. More precisely, this is done through a geometrically-nonlinear structural mechanics solver, which correctly models the nonlinear deformations, but retains the linearity of the constitutive relationships. The chosen structural dynamics software is the `GEBT` program (standing for Geometrically-Exact Beam Theory), freely available at [38] and documented in [39,40]. The software, developed in Fortran, has already been successfully employed on several aeroelastic applications, such as in [41,42]. It is a general-purpose tool designed to address the challenging analysis of highly-flexible, slender structures. The main feature of the approach is that displacements, forces and moments are transferred between the deformed and undeformed beam frames according to exact, nonlinear kinematic relationships involving all the translation and rotation degrees of freedom in space. The nonlinear equilibrium is found iteratively using the Newton-Raphson method. A detailed description of the analytical formulation can be found in References [39,40,43]. The nonlinear aeroelastic analyses are performed by coupling `GEBT` with an in-house developed VLM solver, which has already been presented in [44,45]. The aerodynamic and structural domains are interfaced via the interpolation approach proposed in [46], which is based on radial basis functions. This serves as the highest fidelity tool in this framework for aeroelastic analysis of very flexible wings, and in this work it is used for the static sizing of the main wing and for the simulation of its response to gust encounters. A graphical representation of this VLM-based 3D model is given in Fig. 3, showing some details of the aerodynamic and structural discretizations of a sample wing, as well as the resulting aerodynamic loads distribution on the deformed surface. Finally, it is worth noting that compressibility is taken into account in both the 2D strip theory and the VLM models via the Prandtl-Glauert correction, which is considered valid for steady or quasi-steady flow up to Mach 0.7 [47]. For fully-unsteady aerodynamics (above a reduced frequency of 0.05), some corrections exist in the literature, but they require the definition of several additional coefficients or indicial functions, that introduce additional complexity, uncertainty and computational cost. Fully-unsteady conditions are expected to be relevant here only for flutter analysis, which we address via the 2D strip theory model. As far as this method is concerned, it is known that the adopted approach, that applies the Prandtl-Glauert correction to the lift-curve slope, results in conservative flutter speed predictions [48]. Therefore, such correction was considered sufficient for the purpose of this work.

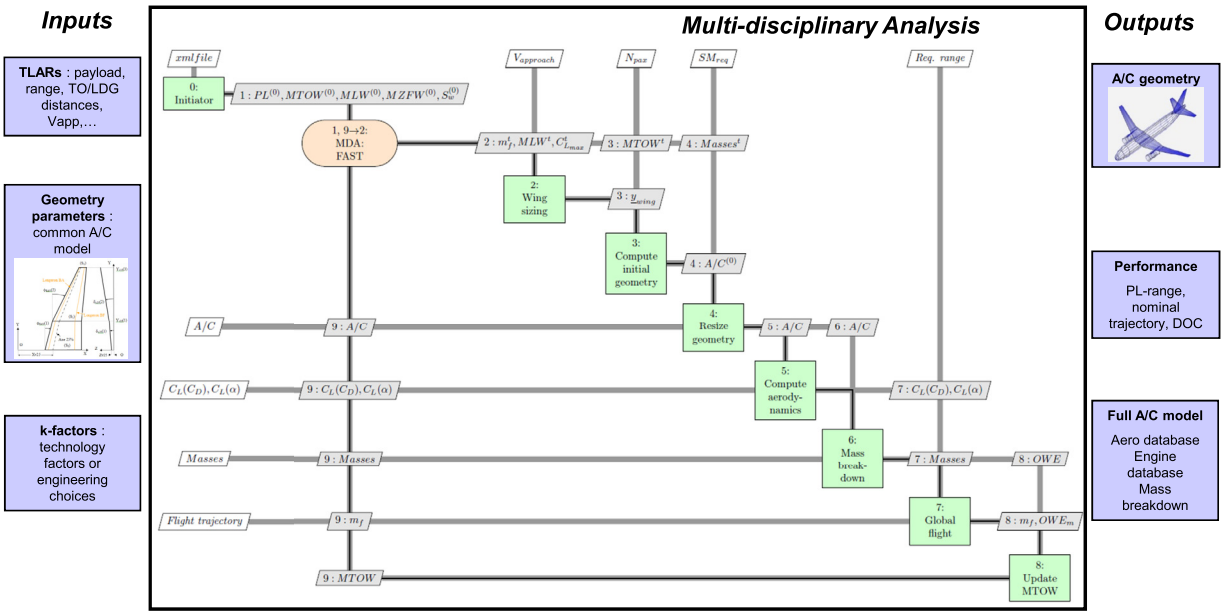

Fig. 4. Structure of the FAST-OAD overall aircraft design suite, from [50].

3.2. Overall aircraft design

The computational framework builds upon the aircraft design tool Fixed-wing Aircraft Sizing Tool, FAST. FAST has been developed by ONERA and ISAE-SUPAERO since 2015 and it is conceived as a quick conceptual design tool to be used either for testing and designing conventional concepts, or in combination with advanced analysis tools for unconventional design explorations. A detailed documentation covering all the main internal processes can be found in [49,26]. The most recent upgrade of the tool has been renamed FAST-OAD (for Overall Aircraft Design) [50], and is today available open-source on GitHub.[1] In its basic formulation, the user specifies a series of TLAR and an initial geometry, and the framework estimates the overall aircraft performance (such as fuel mass, payload range, etc.) through a series of sizing loops involving modular analyses for the key disciplines. These include basic flight mechanics, aerodynamics, structures, propulsion, weight and balance. The original approach is based on a point mass approximation together with semi-empirical equations for performance, weight and aerodynamic predictions. This allows high computational efficiency and accuracy to be achieved as long as traditional concepts are treated. The propulsion module can be based either on a pre-specified dataset, or on an analytical model that provides thrust and fuel consumption as functions of altitude and flight speed [51]. The performance module gathers all the information from the disciplinary modules and performs a time marching simulation of the full mission. Sizing and positioning of components are iteratively updated during the design loops through dedicated geometry, weight and balance modules. Overall aircraft design rules from [52] are used to initially locate the main components, such as wing, tail, landing gear, etc. An overview of the multidisciplinary structure of the tool is given in Fig. 4.

FAST-OAD has recently been used for more advanced studies by interfacing it with physics-based analysis tools to extend its applicability to novel aircraft concepts, such as blended wing-body, distributed propulsion, electric and hybrid propulsion [44,53–55].

[1] https://github.com/fast-aircraft-design/FAST-OAD.

3.3. Optimization approach

Our optimization task relies on a Bayesian Optimization approach using the SEGOMOE toolbox (standing for Super Efficient Global Optimization with Mixture of Experts) by ONERA and ISAE-SUPAERO [19]. The Bayesian optimization is especially convenient when function derivatives are not immediately available, because no derivative needs to be computed through finite differences. Consequently, in such cases of "black-box" functions, the required number of function calls is considerably reduced compared to other approaches. The method leverages on Gaussian surrogate modelling of the objective function and constraints, enhanced by different available adaptive learning strategies. In this work the enrichment process was guided by the Watson and Barnes criterion (WB2) [56] that gives slightly more merit to local search. Constraints were handled by means of Upper Trust Bound [20], which encourages exploration of the feasible domain by combining the mean prediction and the associated uncertainty function given by the Gaussian processes.

3.4. Uncertainty quantification

Early aircraft analysis is inherently affected by aleatory and epistemic uncertainties. With our attention directed to aeroelastic performance estimation at conceptual design level, we include and propagate the most relevant uncertainties onto the desired output performance indicators. We consider the investigation into static sizing loads, flutter speed and dynamic gust loads at wing level, and therefore the uncertainty herein considered is that arising from the approximate methods used during the sizing process to estimate wing structural characteristics.

The off-the-shelf Uncertainpy toolbox [57] was selected for uncertainty quantification and sensitivity analysis and interfaced with the aeroelastic analysis modules. It was a natural choice following its successful use on a previous robust aircraft MDAO application, based on an earlier version of the present framework [45]. The toolbox, originally conceived mainly for computational neuroscience, is easily adaptable to any computational field in that it is a model-independent, open source, Python-based platform. Herein, we summarise only the main features. The sensitivity analysis is addressed by computation of first-order Sobol indices and

total Sobol indices when interactions between the uncertain parameters exist. As far as uncertainty quantification is concerned, it implements both quasi-Monte Carlo methods and Polynomial Chaos Expansions (PCE) using non-intrusive methods. The quasi-Monte Carlo methods employ variance-reduction techniques to reduce the number of model evaluations needed. As for the PCE approach, the orthogonal polynomials are found using the three-term recurrence relation, and the expansion coefficients can be found either through the Tikhonov regularization, belonging to the class of point collocation methods, or by a pseudo-spectral approach based on Leja quadrature and Smolyak sparse grids. The Sobol first and total order methods can be computed directly from the PCE [58]. The output metrics provided are the mean, variance, 5% and 95% percentiles (P_5 and P_{95}) and the Sobol indices. Additionally, some modifications were made to obtain the Probability Distribution Function (PDF) together with any desired percentile.

4. Flexible wing sizing

We describe in detail the structural sizing and optimization process for flexible wings and how this is brought together with the overall aircraft sizing process. First, the approach for the guess initialization of the wing structure is introduced in Section 4.1. The outcome of this initial guess is a simplified 3D wing-box structure. In order to enable the assessment of the aeroelastic performance of the resulting wing, the 3D wing-box model is first reduced into an equivalent beam model. This process is explained in Section 4.2. Once the aeroelastic model is ready, with both the beam model and the VLM aerodynamic model correctly generated and interfaced, the static aeroelastic analysis can be launched to finalize the wing structural sizing, now taking into account the effects of flexibility. The numerical setup for this analysis and the definition of the sizing load case are detailed in Section 4.3. Once the static aeroelastic analysis for the wing structural sizing is clearly defined, Section 4.4 describes how the optimization process is realised to produce the best structural layout, in terms of structural mass, that satisfies the imposed static safety requirements. Two sample optimization cases are also provided.

4.1. Initial sizing of a wing-box structure

The overall aircraft design tool `FAST-OAD`, following a conventional approach, was not designed to encapsulate stress analysis or aeroelastic analysis during the sizing loops. Therefore, it does not handle sufficient information about the structural layout to allow for these types of studies. This fact translated into a gap between the existing design process and the desired extension leveraging on the developed aeroelastic tools. For instance, the aeroelastic models in question need input quantities such as bending rigidity, torsional rigidity, moments of inertia, mass distribution, shear centre location. This information is unnecessary, and therefore unavailable, within the `FAST-OAD` routines. This gap was filled by estimating a simplified wing-box structure, initially sized using simple analytical expressions for loads and stress calculation. This is a common approach in literature when addressing wing aeroelastic sizing and optimization (see for instance [59,37,9]).

The sizing process finds inspiration from [60]. Aeronautical aluminium properties, summarized in Table 2, are assigned to all components. The wing-box geometry is assumed having a rectangular cross section, composed by the three main functional elements: two (identical) spars carrying the shear loads, the skin absorbing the twisting loads and a set of stringers and spar caps resisting bending loads. A schematic representation is given in Fig. 5(a). In addition, ribs are also considered, but only for mass estimation, based on data from the same category of aircraft, and they do not carry any load. The breakdown into the three main functional elements means that the three different kinds of loads - vertical shear, torsional shear and bending stress - are totally assigned to the corresponding structural components: the spars are sized to sustain the total vertical force, the skin to carry the total twisting moment, the stringers to withstand the total bending moment. This separation allows the structure to be quickly sized analytically. As far as the 2D cross-section is concerned, the outer rectangle dimensions are fixed by three outputs from `FAST-OAD`: the two chordwise locations of the front and rear spars, and the average thickness ratio of the aerodynamic profile. The resulting wing-box planform is represented in Fig. 5(b), which refers to the CeRAS baseline wing planform. As the rectangular cross-section is assumed to be perfectly symmetrical, its shear centre is considered located at the rectangle centroid, and therefore the EA is located exactly in the middle of the two spar lines.

Table 2
Material properties for the wing-box components. Values typical of aeronautical aluminium alloy.

Property	Symbol	Unit	Value
Density	ρ_m	kg/m^3	2900
Young's modulus	E	GPa	68.9
Shear modulus	G	GPa	24.0
Yield strength	σ_m	MPa	276
Shear strength	τ_m	MPa	207

With the cross-section perimeter being defined, its layout can be completely described by three additional parameters: the skin thickness, t_s, the total web thickness, t_w (twice the thickness of one spar), and the stringers cross section, A_s. These are illustrated in Fig. 5(a). The stringers are considered equally distributed along the chord, on both the lower and upper surfaces, and they are regarded as longitudinal rods located along the skin, supposed to react the normal stress needed to counteract bending. Therefore, the only parameter that needs to be sized is their total area. Their actual number and shape are not relevant at this stage of the design process. The parameter A_s refers to the sum of all cross section areas of the stringers located on the upper (or lower) surface, so that the total available area equals $2\,A_s$. We found that this functional partitioning approach is more conservative than evaluating an equivalent Von Mises stress at the most stressed point of the cross section, and, despite approximated, it matches satisfactorily with the semi-empirical correlations used in `FAST-OAD`, as it will be shown later. Therefore, we decided to keep this idealization not only for the initial guess of the three variables but also during the wing mass optimization iterations.

The span-wise parameterization is again kept simple, following [60]: the three variables t_s, t_w, A_s are linearly scaled from root in order to reach the minimum technological values at the wing tip. In this way, the structural optimization problem is reduced to three dimensions, corresponding to the three cross section parameters at the wing root, which is assumed to be the most solicited section. A view of the adopted wing-box idealization is given in Fig. 5(c).

It should be noted that only the three main structural responses above are taken into account for sizing the structure and for constraining the optimization. The limits are set by the material yield and shear strengths. Other aeroelastic sizing approaches, such as in [61,37], usually constrain the problem with additional types of failure, such as stringer buckling, panel compression and shear buckling, stringer-panel buckling or crippling, which are not considered here. Instead, secondary failure modes are considered prevented by summing to the primary structure mass an additional weight fraction, estimated by `FAST-OAD`, accounting for appropriate reinforcements and other secondary masses. The main reason for this simplifying choice is that the increased level of detail would require several additional optimization variables, such as

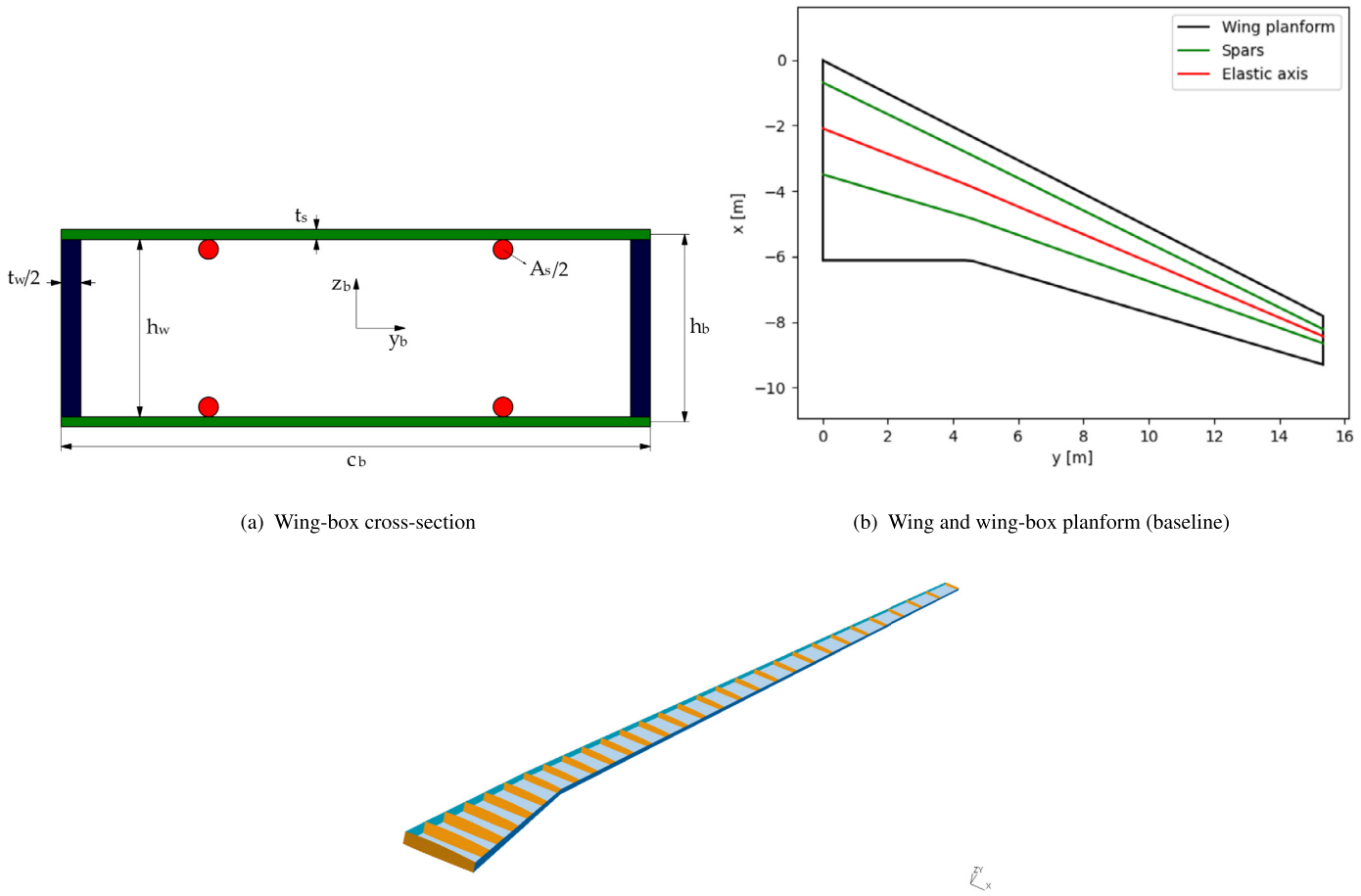

(a) Wing-box cross-section

(b) Wing and wing-box planform (baseline)

(c) 3D wing-box idealization ('stretched $\mathcal{AR}$ -15')

Fig. 5. Wing-box idealization adopted in this work: cross section idealization (a), planform (b) and 3D view of the layout for the CeRAS baseline and for a 'stretched $\mathcal{AR}$ -15' configuration (c).

stringers shape, stringers spacing, ribs number, ribs spacing. This would turn into a much higher computational cost, and a level of detail more appropriate to preliminary than conceptual design. As reinforcements are already taken into account, the added cost of the extended design space would be of marginal use, and would add unnecessary complexity with respect to this first, demonstrative application to robust aeroelastic MDAO. Also, the introduction of one or more additional structural variables and constraints represents a fairly simple modification to the code architecture, and would not bring any substantial change in the philosophy of the approach. It should be noted that the main focus here is the wing structural weight, because of its impact on the mission fuel burn. In this perspective, it is assumed here that the additional constraints would mainly impact the structural layout, in terms of ribs and stringers distribution, with little influence on the overall wing mass. Finally, as it will be shown later, some effects linked to fluctuations in the nominal section properties, due to the remaining uncertainty on the structural configuration, are still accounted for, at least in the evaluation of the aeroelastic reliability constraints. For these reasons, the implementation of additional structural constraints, that would further substantiate the feasibility of the design, is left to future developments, and is not included in the present work.

The initial sizing and weight estimation of the wing-box is achieved by four separate steps, corresponding to skin, web, stringers and ribs sizing. Loads are estimated based on a positive limit load factor $n_L = L/W = 2.5$. Neglecting the contributions of fuselage and horizontal tail, all the lift is supposed to be carried by the wing, and considered acting at the 25% of the mean aerodynamic chord. The overall force and moments are applied to the wing root section, supposed to be the most loaded one, and once its parameters are sized, they are scaled linearly along the span to reach their minimum technological limit at the wing tip. The analytical formulas used are reported in Appendix A.

4.2. Beam model generation for aeroelastic analysis

A wing-box model, albeit simplified, still demands a relatively high computational cost if some aero-structural analysis is to be carried out for conceptual design purposes. This can become especially prohibitive in the present case, where not only multiple optimization and sizing loops are required, but also dynamic analysis and uncertainty quantification are to be performed. Therefore, one further simplifying step is taken here, which is the reduction of the generated wing-box model into an equivalent, 3D beam model. To give an overview of such a model, it is worth listing the main underlying assumptions from the previous discussion:

- The same homogeneous, isotropic aluminium is adopted for all the components;
- Linear elastic behaviour of the material is assumed even if nonlinear displacements are allowed;

- The wing-box has regular rectangular cross sections with two axes of symmetry, their dimensions being derived from the local spars positions and profile thickness;
- The wing-box is the only structural part of the wing to play an active role: no loads or inertia are transferred to or from other parts of the wing;
- The structure is slender, so that vertical and horizontal shear deformations are negligible with respect to the effect of rotation;
- All cross sections rotate and translate rigidly.

These assumptions allow stating the following:

- Only one elastic modulus, E, and one shear modulus, G, are needed, and they are set equal to the standard values available for aeronautical aluminium, reported in Table 2;
- The shear centre of each cross section is located at the centroid of the wing-box rectangle;
- The centre of gravity of each cross section with and without fuel is located at the centroid of the wing-box rectangle;
- Only three main sectional moments of inertia need to be calculated, the products of inertia being zero due to the section symmetry;
- Only the wing-box geometry is needed to completely define the elastic and inertial properties of the equivalent beam;
- The equivalent beam can be conveniently placed along the locus of all centroids of the wing-box.

With these considerations in mind, it is possible to derive all the needed parameters to define the beam model by means of standard analytical relationships, reported in Appendix B.

4.3. Sizing load case definition

With the aeroelastic model ready, the sizing process for the elastic wing is addressed. Wings shall be sized to withstand manoeuvre and gust loads. Manoeuvre loads are treated as steady loads, so that a few static load conditions are selected and applied to the wing. In a preliminary design context, this translates into the selection of one positive and one negative load factor, and several flow conditions determined by the different flight altitudes. Here, in the context of conceptual design, although “enriched”, the static load case scenario is restricted to a single condition. This is defined by a limit load factor of 2.5, and a flight speed corresponding to the dive speed referred to sea-level (EAS). As regulations specify that “the structure must be able to support limit loads without detrimental permanent deformation”, the sizing process here has to ensure that the material yield strength is not exceeded at the prescribed load case. It is important to underline that this condition is here verified only at the wing root, which is the most solicited section.

4.4. Wing structural optimization

The objective function to minimize here is the mass of the wing-box structure W'_{w2}, also referred to as the primary structure, which does not include reinforcements or secondary parts. The strategy adopted is to start with an initial guess of the structural layout, derived as discussed in Section 4.1, and then to run an optimization with SEGOMOE to minimize the structural weight within a design space surrounding the initial guess configuration. This is intended to reduce the search space and therefore speed-up the convergence. In fact, it is expected that high aspect ratio wings require a stronger structure compared to low aspect ratio ones, and therefore it is detrimental to use a unique, wide design space in the two situations.

Consistently with the above initial guess approach, the size of the optimization problem is kept as small as possible by relying only on the three variables t_s, t_w and A_s defined above (see Fig. 5(a)). Again, to eliminate possible additional variables, the lower technological bounds of these three parameters are assigned to the wing tip, and a linear decrease is assumed to define their distribution along the span. Such an hypothesis is believed to be conservative, as in other, more detailed studies on similar aircraft (as in [61]) the slope of this decrease is allowed to change in order to reach the minimum bounds of the parameters before the wing tip, with the effect to further decrease weight. In other cases (such as in [37]) the wing-box parameters at multiple stations are even treated as independent variables. These approaches are powerful and effective for a single wing optimization case, but would require a much higher cost if applied in this work, where many optimization cases are to be addressed. In line with the choice of the three optimization variables, located at the wing root, the only constraints employed are the corresponding bending and shear stresses at that station. Monitoring many stress values all over the beam as additional constraints would represent an increased burden for the structural optimizer, and it is not considered an essential task at this stage. A more detailed optimization approach and a comparison of the computational costs may be the object of future studies.

In the present case, three root loads are considered to constrain the optimization: the torsion shear on the skin, τ_t, the vertical shear on the webs, τ_v, and the bending stress on the stringers, σ_b. They are calculated by the expressions given in Appendix A. The constraints ensure that the material shear strength, τ_m, is not exceeded in the skin and spars at the root section, and that the material yield strength, σ_m, is not exceeded in the stringers (the numerical values are reported in Table 2). As mentioned above, the 3D design space is adaptively bounded for each aircraft configuration depending on the pre-calculated initial guess $[t_{s0}, t_{w0}, A_{s0}]$. The upper bounds for the variables are set to 1.5 times the initial guess values. For the lower bounds, a factor of 0.5 is applied, but for the skin and web thicknesses a comparison with the corresponding minimum technological value is made, and the largest value is retained. The minimum skin thickness is set equal to 2.7 mm, a value commonly assumed for lightning strike requirements [61]. For the spars thickness, the minimum aluminum sheet thickness of 1.2 mm is selected [60]. No technological bounds are applied for the stringers' area. The wing structural optimization problem is summarized in Table 3. Two examples of the sizing and optimization results are given below. In the first one the wing of the CeRAS baseline configuration is adopted as a reference case to validate the approach. Then, the same process is repeated on a higher-aspect-ratio configuration ($\mathcal{AR}$ =15), which will be hereafter referred to as the ‘stretched $\mathcal{AR}$ -15’ configuration.

The mass predictions for the overall structure of the two wings, as well as their different components, are detailed in Fig. 6. Here, the mass fraction corresponding to stringers and spar caps, which mainly sustain bending loads, is labelled as “bending” mass. The mass of skin and spars, whose main function is to react shearing loads, are not separated in FAST-OAD, so they are grouped in the “shear” mass. It is worth reminding that the difference between the total empty weight mass, W_w, and the primary structure mass, W'_w, composed by the skin, spars, stringers and ribs, is the mass of landing gear reinforcements and secondary masses, which is set equal to the value given by FAST-OAD. Fig. 6 shows that the two proposed approaches (the initial guess and the aeroelastic optimization) are in good match with the FAST-OAD sizing results for all the wing sub-parts, especially for the baseline wing (see Fig. 6(a)). As FAST-OAD was finely tuned around the CeRAS baseline, such matching confirms that both the initial guess and the aeroelastic optimization approaches provide realistic results.

Table 3
Definition of the structural optimization problem for the flexible wing.

	Function/quantity	Lower bound	Upper bound
Minimize	Wing structural mass W'_{w2}		
with respect to	Root skin thickness t_s	$\max(0.5\,t_{s0},\, t_{sL})$	$1.5\,t_{s0}$
	Root spar thickness t_w	$\max(0.5\,t_{w0},\, t_{wL})$	$1.5\,t_{w0}$
	Root stringers area A_s	$0.5\,A_{s0}$	$1.5\,A_{s0}$
subject to	$\tau_t < \tau_m$ (material shear strength not exceeded)		
	$\tau_v < \tau_m$ (material shear strength not exceeded)		
	$\sigma_b < \sigma_m$ (material yield strength not exceeded)		

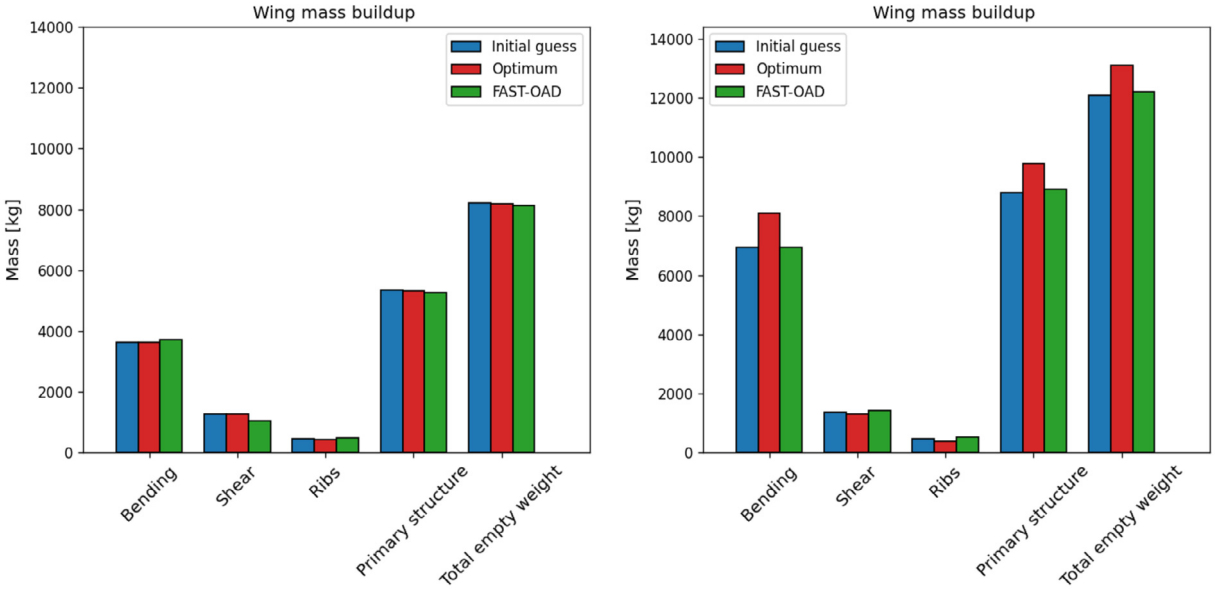

(a) Baseline ($\mathcal{AR}$ =9.5) (b) 'Stretched $\mathcal{AR}$ -15' configuration

Fig. 6. Wing structural mass buildup for the CeRAS baseline (a) and for the 'stretched $\mathcal{AR}$ -15' configuration (b). Three sets of data are compared: the FEM data for the initial guess structural layout (blue), the FEM data for the optimal structural layout (red) and the estimation for the rigid aircraft by `FAST-OAD` (green).

However, the high aspect ratio example (see Fig. 6(b)) shows that, differently from the baseline case, the aeroelastic module is predicting an appreciable difference with respect to the conventional `FAST-OAD` approach, indicating that the latter may not be totally accurate for flexible wings. In particular, the aeroelastic optimization gives a wing-box mass and a total empty-weight wing mass around 11% and 8% higher than the respective values from `FAST-OAD`. The mismatch suggests that the conventional approach may lead to underestimating the loads deriving from wing flexibility, and therefore the structural mass required to sustain them, confirming that the adoption of the proposed aeroelastic approach is a desirable enhancement.

5. Dynamic aeroelastic constraints

5.1. Flutter constraint

We included flutter speed as a dynamic aeroelastic constraint. Both the European and U.S. airworthiness regulations for large aeroplanes impose that the airplane must be free from aeroelastic instability within an envelope enlarged up to 15% in terms of Mach and air speed at all altitudes [62,63]. Here, one single limiting condition is considered, corresponding to the speed threshold of $1.15\,V_D$ EAS (= 200 m/s in the present study), and to a Mach number of 0.6, based on the sea-level speed of sound of 343 m/s. Such conditions fall within the validity range of the adopted methods (see Section 3.1). No other conditions, such as different altitudes and Mach numbers are studied, even though the cruise Mach number is 0.78. This is motivated by the fact that the adopted tools would not capture more complex phenomena such as dynamic shock waves or buffeting that could be involved at high altitude, transonic conditions. Therefore it would be of no use to repeat the same analysis with different, less reliable flow conditions. The verification of such complex conditions and effects must be left to the mode advanced design phases.

Before formulating the flutter probabilistic constraint, a sensitivity study was carried out to identify the parameters that have the highest impact on the flutter instability. Six wing parameters were selected to run the sensitivity analysis: the EA location, a, the offset between the EA and the CG, d, the beam average mass per unit length, μ, the bending and torsional stiffnesses, respectively, EI^A_{yy} and GJ, and the moment of inertia, I_p. It is worth noting that such analysis removes the limiting assumption introduced for the wing optimization loop, where the EA and the CG were both considered coincident with the centroid of the rectangular wing-box. Note also that an important assumption still holds: all these quantities are defined at the wing root, and any change during the sensitivity study is proportionally applied all over the wing span, the proportion being calculated at each station with respect to the local value of the nominal wing-box. The chosen uncertain parameters and their distributions to be used in the flutter sensitivity analysis are reported in Table 4. The results showed a net dominance of two parameters, a and d. These findings can be explained as follows. The EA distance from the aerodynamic cen-

Table 4
Uncertain parameters and corresponding distributions adopted for the flutter sensitivity analysis. All distributions are Gaussian. Symbols denoted with a bar $\bar{(\cdot)}$ represent the nominal values produced by the sizing and optimization process. The symbol σ indicates the standard deviation.

Property	Mean	Standard deviation
Elastic axis location	$\bar{a}$	$3\sigma = 10\%$ chord
CG shift from EA	$\bar{d}$	$3\sigma = 5\%$ chord
Mass per unit length	$\bar{\mu}$	$3\sigma = 10\%\bar{\mu}$
Bending stiffness	$\overline{EI}^A_{yy}$	$3\sigma = 10\%\overline{EI}^A_{yy}$
Torsional stiffness	$\overline{GJ}$	$3\sigma = 10\%\overline{GJ}$
Polar moment of inertia	$\bar{I}_p$	$3\sigma = 10\%\bar{I}_p$

tre of pressure has a direct effect on local twisting moment, which can significantly increase or decrease the local angle of attack, and therefore the local aerodynamic moments. A similar role is played for inertial forces by the CG offset d from the EA. Mass and inertia are less relevant on their own, as the main effect is driven by d. Finally, stiffness has a more direct impact on deformations, but not necessarily on stresses. These results suggest that the robust MDAO process can be addressed by only assigning uncertainty to these two quantities. More details on these results are given in Appendix C.1.

5.2. Gust loads constraints

Concerning gust calculations, a compromise was needed when selecting the tools to be used. The model adopted for flutter predictions was discarded for different reasons. First, the structural model would neglect any nonlinear effect in terms of deformation and pre-stress due to static loads before gust encounter. Also, the implemented unsteady strip theory would not capture three dimensional flow effects around the wing tip. This is not desirable for gust loads evaluations, because the airloads on the outboard wing region have significant impact on the bending loads. Also, structural twist is accentuated towards the wing tip, with a relevant effect on those tip loads, and twist is not modelled in the 2D unsteady strip theory method used for flutter. Finally, discrete gust calculations will be limited to the first wing structural peak frequency, as it will be explained later, corresponding to a reduced frequency of approximately 0.02. Such value is well within the range of 0.0 - 0.05 that is commonly accepted as quasi-steady. Therefore, under such conditions, it is assumed that unsteady aerodynamic effects can be neglected. For these reasons, it is preferred to use a 3D, quasi-steady aerodynamic solver, such as the VLM rather than the 2D unsteady strip theory.

Therefore, the chosen aeroelastic model for gust loads investigations is the same used for the static aeroelastic sizing: the beam model adapted from `GEBT`, coupled with the developed VLM. In particular, the initial static equilibrium is found exactly as discussed in Section 4, searching the nonlinear structural solution. Then, the dynamic analysis is carried out from that nonlinear equilibrium, but this time, at each time step, the structural states are updated according to the linear dynamic incremental solution, derived from the instantaneous aerodynamic, inertial and internal loads. The gust is simulated by adding the local gust speed to the VLM boundary conditions, and it is propagated by translating the gust profile downstream at each time step, at free-stream speed.

The constraints on dynamic gust loads were introduced following again the certification specifications [64,65], and in particular about time-marching discrete gust simulations. Of course verifying full compliance with regulations is definitely out of the scope of this work, and in general of any conceptual design task. Here, regulations are just used as a reference to define realistic design constraints, and no attempt is made to enforce a thorough assessment of compliance. The design conditions for gust encounters

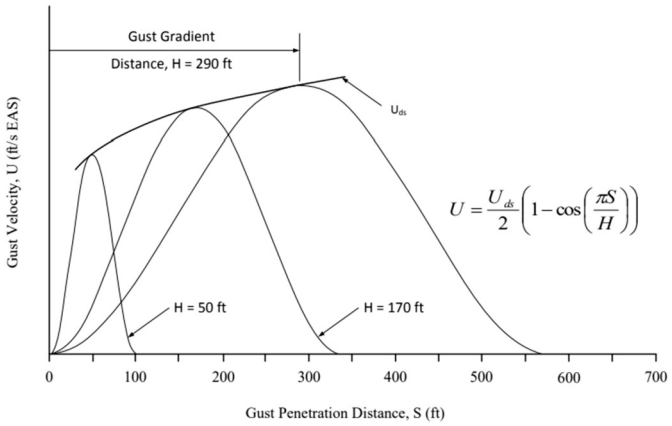

Fig. 7. Typical '1-Cosine' design gust velocity profiles, from the FAA Advisory Circular 25.341-1 [66].

are evaluated with respect to steady, 1-g level flight. Here, cruise speed is used, expressed in equivalent sea-level conditions. For the present baseline, this translates into a density of ρ = 1.225 kg/m^3, a flight speed of 135 m/s and a Mach number of 0.4, again based on the standard speed of sound at sea level of 343 m/s. Only positive (upwards) gust profiles are taken into account. These are defined according to the typical '1-Cosine' shape illustrated in Fig. 7. The desired simulation output is the time history of the same three structural loads that are employed as constraints during the static structural optimization. These are the normal stress on the stringers due to bending, σ_b, the vertical shear stress on the spars due to vertical shearing forces, τ_v, and the shear stress on the skin due to twist, τ_t. Consistently with the static structural optimization approach, discussed in Section 4.4, the quantities monitored are only the maximum absolute stresses at the wing root, and the imposed conditions are that these do not exceed the material strength of Table 2.

In order to limit the computational cost of such simulations during the MDAO, a simplifying choice was made here to restrict the constraints evaluations to one single gust case, in terms of amplitude and frequency. As high aspect ratio wings are expected to suffer gust loads more than low-aspect-ratio ones, such condition was selected corresponding to the most critical gust found for the 'stretched $\mathcal{AR}$ -15' configuration introduced previously. A stricter approach would demand at least one frequency analysis to be run for each candidate configuration to identify its specific peak frequency. However, even frequency analysis leaves some room for uncertainty, as it only captures the steady state response, without providing information about the transient response. This step was not taken here for simplicity, although it would not require much effort to be implemented in future developments. Instead, it was decided to base the gust loads constraints on one single gust input of frequency 1.8 Hz, corresponding to the peak frequency of the 'stretched $\mathcal{AR}$ -15' wing. This choice was arbitrary, and motivated only by the fact that the $\mathcal{AR}$ =15 lays just above the mean of the $\mathcal{AR}$ range considered in the following MDAO (8 to 20). With this limitation, the complete verification of safety is left outside the optimization process, and to be assessed only for the optimal candidate.

As for the flutter speed, a sensitivity analysis was performed over the baseline and the 'stretched $\mathcal{AR}$ -15' configuration to determine which of the six parameters in Table 4 have a significant impact on gust loads. The results showed that only the elastic axis location a plays a decisive role, justifying its uncertainty propagation into gust loads constraints during the overall MDAO study. To explain this outcome, the same reasoning developed for the flutter sensitivity analysis can be here applied, with the difference

Table 5
Definition of the MDAO problem for the flexible aircraft with reliability constraints on flutter speed and gust loads.

	Function/quantity	Range/distribution	Propagated to
Minimize	Fuel mass		
with respect to	Aspect ratio	[8.0 , 20.0]	
	Taper ratio	[0.25, 0.35]	
	Kink span ratio	[0.2 , 0.4]	
with uncertainty on	EA location a	Normal ($\mu = \bar{a}$, $3\sigma = 10\%$ chord)	Flutter, gust
	CG to EA offset d	Normal ($\mu = 0$, $3\sigma = 5\%$ chord)	Flutter
subject to	$P(V_f > 200\,\text{m/s}) > 95\% \Rightarrow c(\hat{V}_f) > 0$		(see Equation (1))
	$P(\sigma_b^{\text{gust}} < \sigma_m) > 95\% \Rightarrow c(\hat{\sigma}_b) > 0$		(see Equation (2))
	$P(\tau_v^{\text{gust}} < \tau_m) > 95\% \Rightarrow c(\hat{\tau}_v) > 0$		(see Equation (3))
	$P(\tau_t^{\text{gust}} < \tau_m) > 95\% \Rightarrow c(\hat{\tau}_t) > 0$		(see Equation (4))

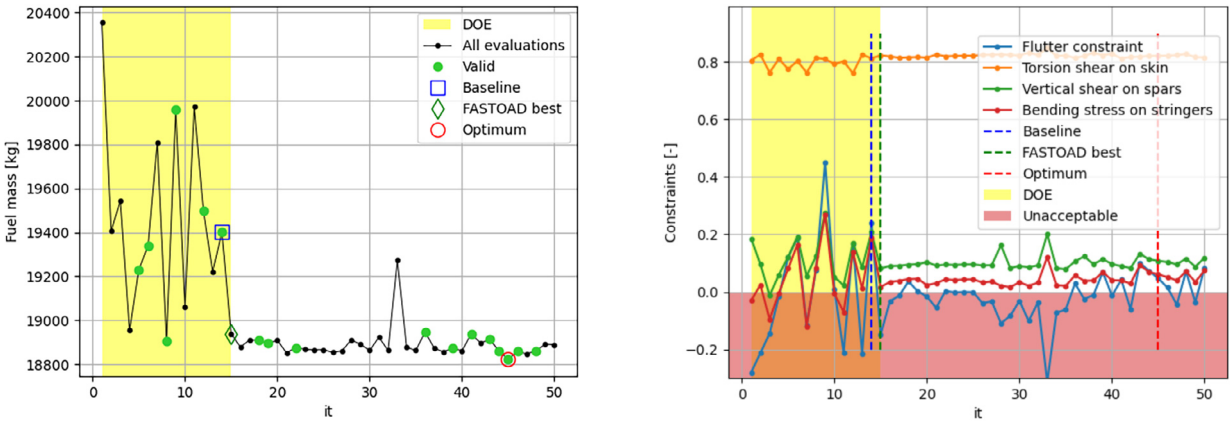

(a) Fuel mass objective

(b) Flutter speed and gust loads constraints

Fig. 8. MDAO process for flexible aircraft under reliability constraints on flutter speed and gust loads. Evolution of the current best fuel mass (a) and the corresponding flutter and gust loads constraints (b) through the SEGOMOE optimization iterations.

that apparently the CG offset d is less important at the simulated gust conditions because the frequency is not high enough to trigger strong inertial loads. Again, more details are reported in Appendix C.2.

6. Optimization results

This section reports the results for a demonstrative MDAO application over the CeRAS baseline introduced in Section 2. The objective to minimize is the mission fuel mass. The design space is limited to three design variables describing the wing planform shape: the aspect ratio, $\mathcal{R}$, the taper ratio, t_r, and the kink position, or span ratio, k_{sr}. The optimization is constrained by reliability constraints on the flutter speed and gust loads, as discussed in Sections 5.1 and 5.2. The output flutter speed distribution, $\hat{V}_f$, is computed after assigning uncertainty to the two parameters with largest Sobol's indices, the EA location a and its distance from the CG axis d. Gust loads distributions are derived by considering only the input uncertainty to the EA location. After a preliminary study, it was found adequate to start the optimization process on an initial Design of Experiments (DOE) of 15 design points, chosen via a Latin Hypercube Sampling (LHS) algorithm, followed by 35 optimization iterations. The problem definition is summarized in Table 5. The tracking of the optimization process is given in Fig. 8. For an easier comparative reading, the plotted constraint values are expressed in normalized form, as defined in Equations (1) to (4).

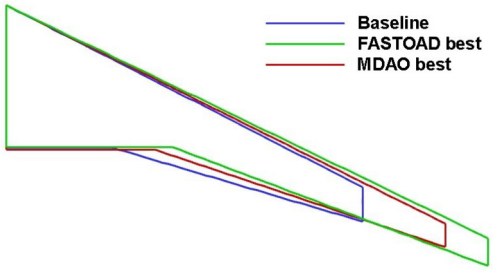

Fig. 9. Best wing planform from the MDAO results under flutter speed and gust loads reliability constraints. The baseline and the best planform from the FAST-OAD rigid aircraft optimization are also reported for comparison.

$$c(\hat{V}_f) = \frac{P_5(\hat{V}_f) - 200}{200} \tag{1}$$

$$c(\hat{\sigma}_b) = \frac{\sigma_m - P_{95}(\hat{\sigma}_b)}{\sigma_m} \tag{2}$$

$$c(\hat{\tau}_v) = \frac{\tau_m - P_{95}(\hat{\tau}_v)}{\tau_m} \tag{3}$$

$$c(\hat{\tau}_t) = \frac{\tau_m - P_{95}(\hat{\tau}_t)}{\tau_m} \tag{4}$$

The optimal candidate is represented in Fig. 9, and its numerical details are given in Table 6. These are compared with the optimal configuration found using a traditional approach, based on the rigid aircraft assumption, performed by use of FAST-OAD alone,

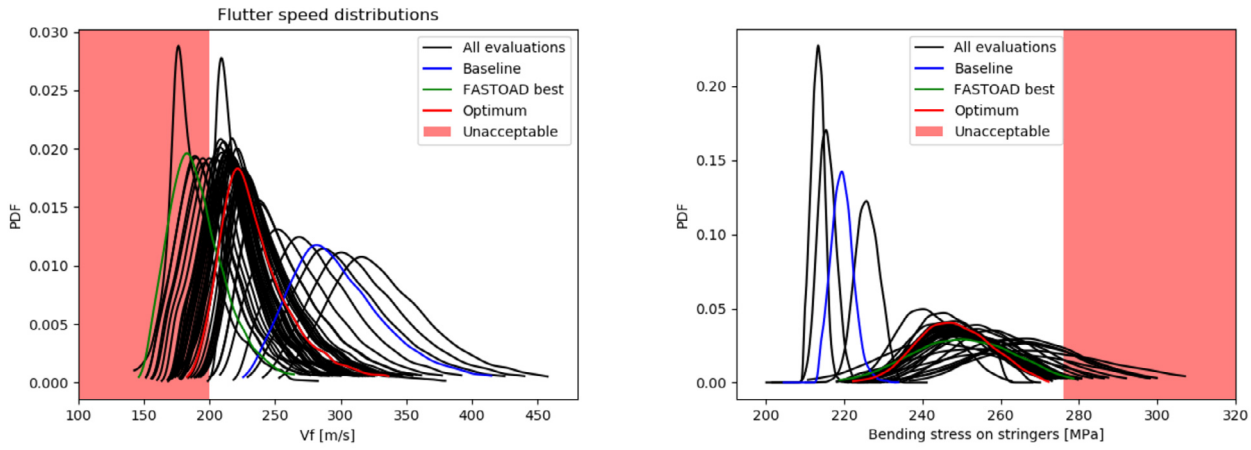

(a) Flutter speed distributions

(b) Gust bending stress distributions

Fig. 10. MDAO process for flexible aircraft under reliability constraints on gust loads. Juxtaposition of all evaluated flutter speed distributions (a) and gust bending loads distributions (b) during the optimization process.

Table 6
Best points from the rigid and flexible aircraft optimization results, compared against the CeRAS baseline data.

Case	$\mathcal{AR}$	t_r	k_{sr}	Fuel mass
Baseline (CeRAS)	9.5	0.31	0.37	19,400 kg
FASTOAD best (rigid A/C)	14.9	0.35	0.4	18,714 kg
MDAO best (Flexible A/C)	13.0	0.25	0.4	18,821 kg

without including any aeroelastic modules and constraints. A few aspects are worth commenting. To begin with, at a first glance it is quite evident that the optimizer is efficient at approaching the optimal region, as the fuel mass values in Fig. 8(a) drops close to the optimum immediately after the computation of the DOE. An interesting observation is about the candidate that scored best in the rigid aircraft optimization based on `FAST-OAD`. It is identified by a green diamond in Fig. 8(a), and by a green dashed line in Fig. 8(b). In fact, under the new approach where aeroelasticity is taken into account, this configuration not only violates the flutter constraint, but it does not even appear as efficient as predicted from the basic `FAST-OAD` analysis in terms of fuel consumption. Indeed, its fuel mass is increased to above 18,900 kg, around 1.3% higher than what estimated with the rigid aircraft approach. This is due to the static flexible wing sizing process that required a stronger and heavier wing structure in order to resist the high loads. For this reason, the candidate no longer results optimal. The best configuration, instead, was found in correspondence of the lower aspect ratio of 13 (see again Table 6). Its figure of merit amounts to 18,800 kg, just above the 18,700 kg of the best configuration from the rigid aircraft approach of `FAST-OAD`.

It is interesting to note that together with the aspect ratio, also the optimal taper ratio changed with respect to the rigid aircraft optimization, shifting from 0.35 to 0.25. This drop is another effect of the aeroelastic sizing, which penalizes the shift outboard of the aerodynamic loads caused by high taper ratios. In fact, at a lower taper ratio the reduction of bending loads, which translates into a lighter structure, compensates the loss in aerodynamic efficiency. As far as the kink span location is concerned, the outboard location of 0.4 benefits to the aeroelastic behaviour of the wing, because it concentrates a larger fraction of the wing area closer inboard, contributing to loosen bending loads and thus reducing the required airframe weight.

As far as constraints are concerned, it can be noted from Fig. 8(b) that the most stringent one is the flutter requirement, as a large number of constraint violations can be observed both during DOE evaluation and the optimization process. Concerning the gust loads, a significant difference is found between the shearing stress constraints and the other two: the direct and vertical stress safety margins oscillate between 0% and 30%, with the optimum featuring around 10% for both of them, whereas the torsion shear stress is always largely safe, with margins above 80%. This is an expected outcome, considering what discussed in Section 4.4, confirming that the estimations done with the proposed method can be considered conservative in terms of structural mass allocation.

Another aspect worth observing is the results of the propagation of uncertainty on the flutter speed during the optimization iterations. The output distributions, in form of PDFs, for all the candidates evaluated during the optimization process are collected in Fig. 10(a). These help gaining a better understanding of the reliability constraint mechanism. Any acceptable configuration must have less than 5% probability of experiencing flutter below 200 m/s. The figure highlights in particular three interesting candidates. The first one is the baseline (in blue): its distribution is quite far above the limit, with practically zero probability of developing flutter below the imposed threshold. Conversely, the best rigid configuration found with `FAST-OAD` alone (in green) evidently violates the constraint, with its distribution laying mostly below the 200 m/s limit, featuring more than 60% probability of developing low-speed flutter. Therefore, while the baseline could be labelled as “excessively” safe, the other would be excessively unsafe. Consistently with this reasoning, the optimum is found in between the two excesses: its distribution, highlighted in red, is closer to the dangerous region, but with only around 4% probability of having an unacceptable flutter speed, proving therefore to be safe “enough” with respect to the prescribed constraint. Another interesting fact emerging from those plots is that low aspect ratio configurations, whose PDFs are located on the right side with higher flutter speeds, show wider distributions compared to high aspect ratio configurations, concentrated on the left side. This outcome, not completely intuitive, demonstrates that despite having in general a greater aeroelastic stability, low aspect ratio wings appear to be more sensitive to structural changes. On the other hand, slender wings are less stable in terms of flutter, but their behaviour seems somewhat more predictable. This is likely due to the fact that the uncertainty is given in percent-

age of the root chord, which translates into higher absolute values for low-aspect-ratio wings (low span and large root chord) compared to high-aspect-ratio ones (long span and small root chord).

In a similar manner, it is interesting observing the output distributions of the gust loads during the optimization evaluations. In particular, the PDFs of the bending loads, the most relevant ones, are reported in Fig. 10(b). As seen in the previous case with the flutter reliability constraint, the baseline configuration is confirmed to be largely away from the dangerous region (its distribution is highlighted in blue). On the other hand, both the robust optimum and the rigid optimum, with their higher aspect ratios, are much closer to the unacceptable region, although none of them demonstrates any significant probability of structural failure. Contrary to the flutter constraint, it can be noted that this time the high aspect ratio configurations, whose distributions are located on the right part of the plots (towards higher loads), prove to be also the most sensible to the structural variations: the more slender the wing, the wider its distribution and therefore the larger the uncertainty and the risk of structural failure.

7. Parametric studies: aspect ratio and aeroelastic reliability constraints

One clear outcome is that the rigid aircraft optimization provides an optimistic solution compared to the flexible aircraft MDAO, with the former giving a fuel burn prediction around 100 kg lower than the flexible aircraft process and a quite different optimal design, especially in terms of $\mathcal{AR}$ (see Table 6). As the other two variables revealed a less pronounced and less relevant impact on the fuel burn, it is interesting here to focus on the fuel-vs-$\mathcal{AR}$ relationship. In particular, it is useful to compare the one-dimensional evolution of the fuel mass with respect to the aspect ratio, obtained from both the rigid and flexible aircraft sizing approaches. This was done by setting the two remaining variables to the corresponding optimal values, $t_r = 0.25$ and $k_{sr} = 0.4$. The resulting curves are plotted in Fig. 11. The two curves, originally coincident and then separating at around $\mathcal{AR}$ = 12.5, have two different minima. In particular, the FAST-OAD curve results smoother and has a distinctly identifiable minimum at $\mathcal{AR} \approx 15$. The initial descending trend of the fuel-vs-$\mathcal{AR}$ curve is explained by the fact that in that range the improvement in aerodynamic efficiency overcomes the impact of airframe weight increase required by slender wing structures, with a positive overall impact on fuel consumption. However, with increasing $\mathcal{AR}$, the weight penalty, due to the need for stronger wing structures to sustain higher and higher bending loads, starts to prevail over the aerodynamic benefits. This causes a gradual trend inversion after the optimal $\mathcal{AR}$ of 15, where the fuel mass curve exhibits a positive slope.

The flexible aircraft curve starts fluctuating after departing from the rigid aircraft curve, generating an irregular, plateau-like region between $\mathcal{AR}$ 12.5 and 15 where a minimum is not clearly recognizable. Before this region, the two curves coincide because the wing mass predictions of FAST-OAD and of the aeroelastic sizing module differ by less than the imposed tolerance of 2%. Therefore, in these cases the overall aircraft resizing is not required, and the fuel mass prediction remains unchanged. When the wing mass difference exceeds 2%, the resizing occurs and the two curves separate. The plateau of the flexible aircraft curve is physically explained by the fact that there is an aspect ratio range where the gain in fuel burn due to improved aerodynamic efficiency of more slender wings is counterbalanced by the increase in structural weight, with no net positive or negative impacts. The irregular trend in this region is characterized by fluctuations

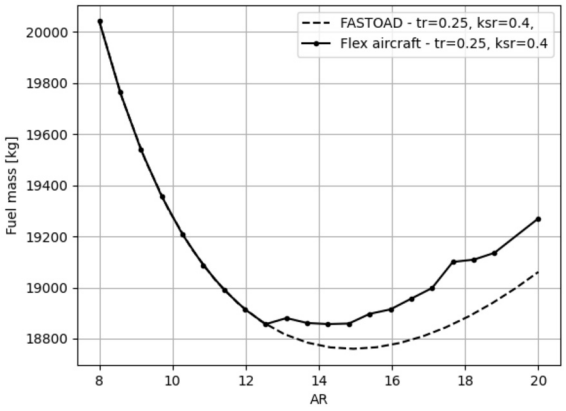

Fig. 11. One-dimensional tracking of the fuel-vs-$\mathcal{AR}$ relationship over the studied space. The two curves correspond to the rigid aircraft sizing process obtained with FAST-OAD alone (dashed line), and to the flexible aircraft approach enabled by the developed methods (solid line). The taper ratio and kink span ratio are fixed to $t_r = 0.25$ and $k_{sr} = 0.4$.

Table 7
MDAO under flutter and gust loads reliability constraints. Optimization results corresponding to different safety increments applied on the constraint definitions.

Safety factor	$\mathcal{AR}$	t_r	k_{sr}	Fuel mass (kg)
0%	13.0	0.25	0.4	18,821
8%	12.0	0.25	0.4	18,912
10%	11.5	0.25	0.4	18,977

of fuel mass in the order of 20-40 kg. Their presence is to be attributed mainly to the 2% tolerance mentioned above, which ensures consistency between the sized wing and the rest of the aircraft.

Another interesting aspect to discuss is the role of the enforced aeroelastic constraints. The optimal aspect ratio $\mathcal{AR}$ =13.0 represents realistically the true minimum of the flexible-aircraft fuel-vs-$\mathcal{AR}$ curve of Fig. 11. This suggests that the prevailing driver is the physical dependence of the fuel with respect to the three variables, and that the constraints are never strict enough to affect the minimization. Nevertheless, this lack of impact is only case-dependent, and a small change in the constraint definition may turn into a totally different optimization outcome. For example, one can imagine that a safety factor is to be imposed on the thresholds for flutter speed and gust loads. This would translate into an upward shift of the unacceptable region, shaded in red in Fig. 8(b). The offset would be equal to the imposed safety factor. To give an idea of what the impact of such a move would be, three cases were compared, corresponding to three different safety factors: 0% (no increased safety, same condition as the discussed examples), 8% and 10%. The effects are shown in Fig. 12. Here, the case with no safety increase is reported first (Figs. 12(a) and 12(b)), corresponding exactly to the optimization case already discussed in Section 6. It can be seen that the optimal aspect ratio region is only marginally impacted by the constraints, and the minimization results would be the same even without enforcing any constraint. The introduction of a safety factor would translate into an upward shift of the unacceptable region (shaded in red) with respect to the one of Fig. 12(a). The offset would be equal to the imposed safety factor. When a factor of 0.08 is considered (Figs. 12(c) and 12(d)), the optimal region in the fuel-vs-$\mathcal{AR}$ space is no longer compliant, and the optimum starts to depend on the severity of the enforced constraints. Both the flutter speed and the gust bending loads show an active role. Increasing the safety factor to 0.1 (Figs. 12(e) and 12(f)) accentuates this trend, showing even less valid candidates, triggering

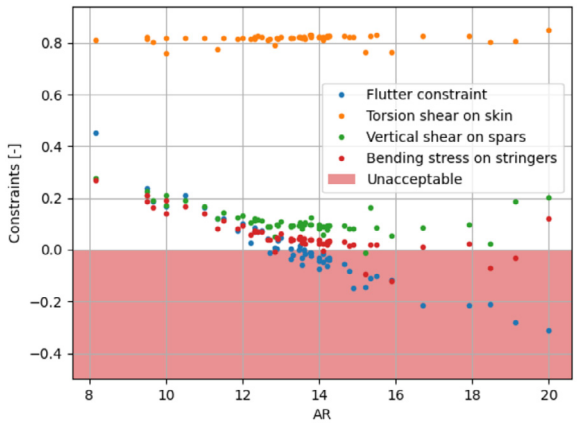

(a) No safety factor - Constraints vs $\mathcal{AR}$

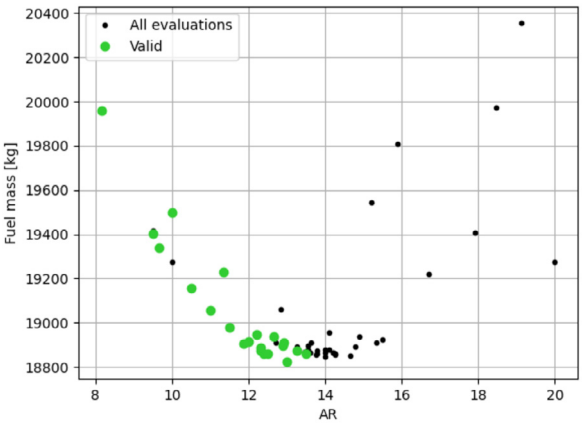

(b) No safety factor - Fuel vs $\mathcal{AR}$

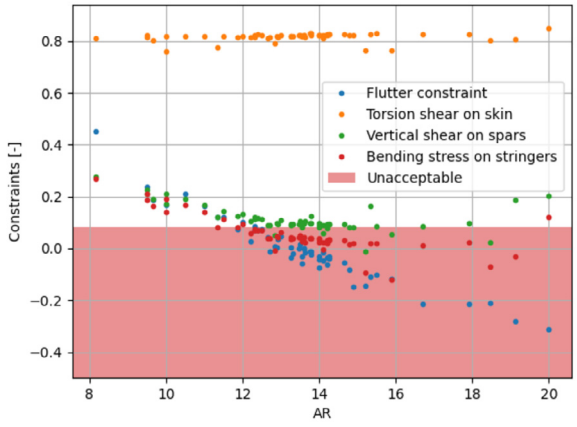

(c) 8% safety factor - Constraints vs $\mathcal{AR}$

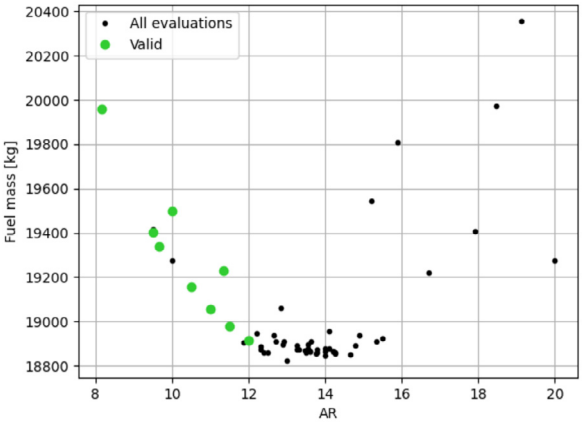

(d) 8% safety factor - Fuel vs $\mathcal{AR}$

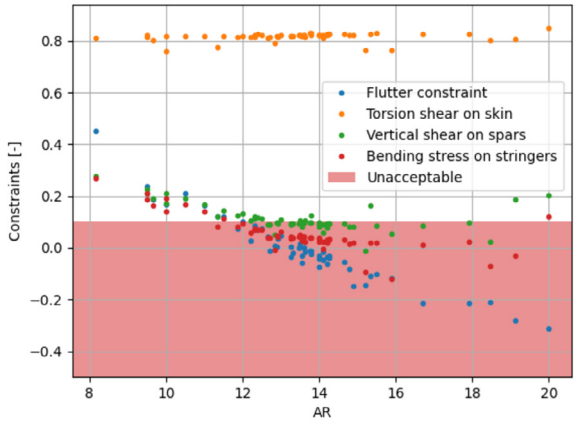

(e) 10% safety factor - Constraints vs $\mathcal{AR}$

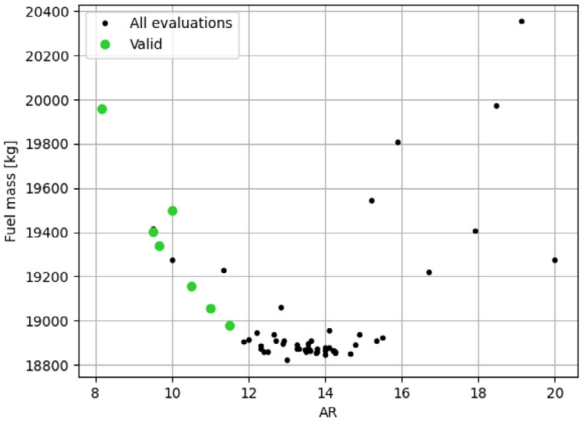

(f) 10% safety factor - Fuel vs $\mathcal{AR}$

Fig. 12. Examples showing the impact of introducing a safety factor in the reliability-constrained MDAO. For each case, the scatter plots of the constraints-vs-$\mathcal{AR}$ and fuel-vs-$\mathcal{AR}$ distributions are reported. The first case (a and b) has no safety factor, corresponding exactly to the MDAO case number 6 discussed above; the second and third cases correspond respectively to a safety factor of 8% (c and d) and 10% (e and f). The safety factor is applied to all constraints, and its effect is highlighted by different red-shaded areas in the left Figures, as well as by different numbers of valid points, highlighted in green in the right figures.

also the vertical shear constraint and further reducing the optimal aspect ratio. The different numerical results are collected in Table 7, and a graphical representation of the corresponding wing geometries is given in Fig. 13. The optimal fuel mass would in-

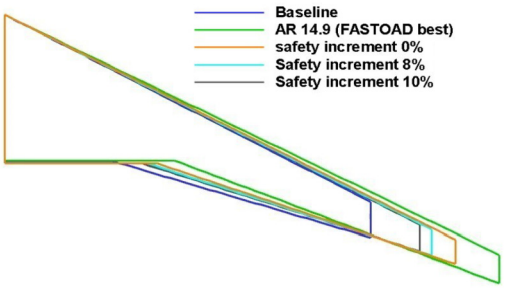

Fig. 13. Best wing planforms corresponding to different safety increments applied on the constraint definitions. The baseline and the best planform from the FAST-OAD rigid aircraft optimization are also reported for comparison.

crease up to about 18,980 kg, more than 150 kg above the loosely constrained optimization, and the best aspect ratio would correspondingly decrease from 13 to 11.5. It is worth noting that a similar effect would originate by an increase in the input uncertainty level.

8. Conclusions and perspectives

We presented a computational framework for the robust multidisciplinary analysis and optimization of flexible aircraft, with applications in the conceptual design phase. The specific case study involved the wing planform optimization of the CeRAS baseline for fuel mass minimization over a fixed mission. Structural flexibility was taken into account for the main wing, which is considered the only element to undergo significant static and dynamic deformations. Uncertainty was attributed to a few structural parameters (the location of the wing elastic and centre-of-gravity axes) and propagated to the constraints on flutter speed and gust loads. The application is a prototype optimization under dynamic aeroelastic reliability constraints.

The choice of our stochastic constraints is not defined by airworthiness regulations, and therefore their choice is somewhat exemplary. It was shown that the optimization results under aeroelastic reliability constraints are indeed dependent on how restrictive the probabilistic requirements are. In general, they have the potential to significantly change the design outcome. For example, it was found that increasing the safety threshold for flutter speed and gust loads by 8 or 10%, respectively, makes the aeroelastic constraints (especially flutter and bending gust loads) much more active, with the effect of reducing the best allowable aspect ratio down to 12.5 or 11.5, and further reducing the fuel mass gain to 2.5% or 2.1%. Results were compared against those for a conventional rigid aircraft design approach, and the main differences were highlighted and discussed. In particular, it was found that the conventional approach can produce dangerous non-conservative results, as its predictions were too optimistic both with respect to the fuel mass objective function, and to the aeroelastic safety of the optimal configuration.

The proposed methodology, therefore, offers a valuable opportunity to address the conceptual design of novel, high aspect ratio aircraft configuration. In fact, it allows to effectively handle aeroelasticity via physics-based tools, with at the same time enabling the designer to perform reliability studies taking into account the unavoidable uncertainty affecting the early design of unconventional concepts. This demonstrative work paves the way to further applications on more disruptive configurations, such as strut-braced wings or box wings. Investigations could also be extended to larger design spaces and number of constraints without requiring any software update. Furthermore, the models could be easily refined to include additional information, for example about engine mass and inertia or control surfaces for loads alleviation. The introduction of computationally-affordable uncertainty quantification additionally paves the way for future novel approaches (up to certification) based on non-deterministic criteria.

Declaration of competing interest

The authors declare that they have no known competing financial interests or personal relationships that could have appeared to influence the work reported in this paper.

Data availability

No data was used for the research described in the article.

Appendix A. Wing-box sizing formulas

This Appendix gives the analytical relationships used for the initial guess sizing of the wing-box structure.

A.1. Skin sizing

The skin is supposed to withstand the torsional moment, estimated as:

$$M_t = \frac{1}{2}\rho V^2 \frac{S}{2} c_{\text{mgc}} C_m + \frac{L}{2}\frac{y_{\text{mgc}}}{\cos\Lambda_{1/4}} \tag{A.1}$$

where y_{mgc} is the location of the mean geometric chord along the y body axis, which divided by the cosine of the quarter chord sweep angle $\Lambda_{1/4}$ gives the arm in the x direction generated by the sweep.

The thickness needed to withstand the limit loads is found by inverting the Bredt's formula for thin-walled cross sections:

$$\tau = \frac{|M_t|}{2\,\Omega_{wb}\,t_s} \quad \Rightarrow \quad t_s = \frac{|M_t|}{2\,\Omega_{wb}\,\tau_m} \tag{A.2}$$

where Ω_{wb} is the wing-box cross section area, that for the present rectangular shape is simply given by the product of its two dimensions c_b and h_b. These are obtained from the FAST-OAD outputs: the former is known from the front and rear spar positions, the latter is derived from the profile thickness ratio, by applying a reduction factor of 0.9. The skin thickness is subject to a lower bound dictated by lighting strike requirements, imposing a minimum thickness commonly set to 2.7 mm (as from [61]).

A.2. Web sizing

With a total vertical force of $n_L W/2$ applied on each wing, neglecting the contributions of fuselage and tail, the maximum shear stress at the root section is:

$$\tau = \frac{3}{2}\frac{n_L W}{h_b\,t_w} \tag{A.3}$$

The required thickness is therefore:

$$t_w = \frac{3}{2}\frac{n_L W}{h_b\,\tau_m} \tag{A.4}$$

The lower bound for the spar thickness is set to the minimal technological limit of 1.2 mm, following [61].

A.3. Stringers sizing

The wing stringers are sized to react the whole wing bending moment generated by lift. The overall cross-sectional area at wing root is here denoted as $2\,A_s$, with A_s being the area located on the

upper and lower skin, in a specular fashion. Therefore, considering half of the total lift applied at the mean geometric chord, the total bending moment at root, and the required stringers area to counteract it are as follows:

$$M_b = \frac{n_L W}{2} y_{\text{mgc}} = \sigma A_s h_b \quad \Rightarrow \quad A_s = \frac{\frac{n_L W}{2} y_{\text{mgc}}}{\sigma_m h_b} \tag{A.5}$$

A.4. Ribs sizing

For the ribs sizing, an approximate estimation is made by assigning them half the local thickness of one spar, considering the same rectangular cross-section of the wing box, and a spacing of about 60-70 cm (as from [37,61]). The higher value of 70 cm was adopted here.

A.5. Reinforcements and secondary parts

This mass is here set equal to the value estimated by FAST-OAD, where a statistical regression is adopted from [52]. Here, the expressions for landing gear reinforcements mass m_r and secondary parts mass m_s are in the forms:

$$m_r = c_1 k_1 (\text{MLW})^{c_2} \tag{A.6}$$

$$m_s = c_3 k_1 (\text{MTOW})^{c_4} S_{\text{PF}} c_5 \tag{A.7}$$

where the coefficients c_i are fixed coefficients, k_1 depends on the number and location of the engines, MLW and MTOW are the Maximum Landing Weight and Maximum Take-Off Weight, respectively, and S_{PF} is the surface of the overhanging wing.

Appendix B. Beam properties derivation

This Appendix describes the calculation of the structural parameters needed to define the present beam model, according to the mentioned assumptions.

The cross-sectional area A is simply given by summing the area of all the wing-box components. With reference to the wing-box parameters illustrated in Fig. 5(a), that gives:

$$A = c_b (h_w + 2 t_s) - h_w (c_b - t_w) + 2 A_s \tag{B.1}$$

With the approximation of thin walls and constant shear flow across the thickness of shell and spars, the torsion constant of the present rectangular cross-section is expressed as:

$$J = \frac{t_s t_w h_b^2 (c_b - t_w/2)^2}{c_b t_s + h_b t_w/2 - t_s^2 - t_w^2/4} \tag{B.2}$$

The two area moments of inertia of the wing-box cross section are given by:

$$I^b_{yy} = \frac{1}{12}\left[c_b (h_w + 2 t_s)^3 - (c_b - 2 t_s) h_w^3\right] + A_s (h_w/2)^2 \tag{B.3}$$

$$I^b_{zz} = \frac{1}{12}\left[(2 t_s + h_w) c_b^3 - h_w (c_b - 2 t_s)^3\right] + A_s (c_b/4)^2 \tag{B.4}$$

The wing-box polar moment of inertia is simply obtained by:

$$I^b_p = I^b_{yy} + I^b_{zz} \tag{B.5}$$

Appendix C. Aeroelastic sensitivity results

This Appendix summarizes the sensitivity analysis results for the baseline and 'stretched $\mathcal{AR}$ -15' wings, revealing the impact of the main structural model parameters, listed in Table 4, on the flutter speed (Appendix C.1) and on the gust loads (Appendix C.2).

Table C.8
Main statistical figures from the sensitivity analysis and uncertainty quantification on the flutter speed for the baseline configuration. The highest Sobol indices, revealing the most impacting parameters, are highlighted in bold.

Distribution properties							
Mean	264 m/s						
Standard deviation	39 m/s						
5th percentile (P_5)	221 m/s						
Sensitivity indices							
	a	d	μ	EI	GJ	I_p	Sum
Sobol first	**0.67**	**0.25**	1.4e-5	1.9e-5	1.0e-2	1.6e-4	0.93
Sobol total	**0.73**	**0.32**	8.6e-4	7.2e-4	1.2e-2	1.0e-3	1.06

Table C.9
Main statistical figures from the sensitivity analysis and uncertainty quantification on the flutter speed for the 'stretched $\mathcal{AR}$ -15' configuration. The highest Sobol indices, revealing the most impacting parameters, are highlighted in bold.

Distribution properties							
Mean	230 m/s						
Standard deviation	35 m/s						
5th percentile (P_5)	192 m/s						
Sensitivity indices							
	a	d	μ	EI	GJ	I_p	Sum
Sobol first	**0.55**	**0.32**	8.3e-5	9.7e-5	9.7e-3	6.6e-4	0.88
Sobol total	**0.65**	**0.43**	6.4e-3	5.9e-3	2.0e-2	8.3e-3	1.12

Table C.10
Main statistical figures from the sensitivity analysis and uncertainty quantification on the gust-induced bending loads at wing root for the baseline configuration. The highest Sobol indices, revealing the most impacting parameters, are highlighted in bold.

Distribution properties							
Mean	220 MPa						
Standard deviation	3 MPa						
95th percentile (P_{95})	226 MPa						
Sensitivity indices							
	a	d	μ	I	J	I_p	Sum
Sobol first	**0.74**	0.03	0.12	0.08	0.03	7.8e-6	1.0
Sobol total	**0.74**	0.03	0.12	0.08	0.03	3.0e-5	1.0

C.1. Flutter speed

As expected, the sensitivity study on flutter speed reveals that the 'stretched $\mathcal{AR}$ -15' distribution is much closer to the unacceptable region (shaded in red) than the baseline wing (see Figs. C.14(a) and C.14(b)). It also emerges that for both wings, out of the six uncertain parameters, only two of them, namely the EA position a and its distance from the CG d, have a major impact on the flutter speed, at least with the assumed input distributions. The corresponding metrics and sensitivity indices for the two distributions are reported in Tables C.8 and C.9.

C.2. Gust loads

Similarly to what seen for the flutter study, and as expected, the sensitivity analysis on gust bending loads shows that the 'stretched $\mathcal{AR}$ -15' distribution is again the most critical (see Figs. C.15(a) and C.15(b)). The shear loads are less severe and the corresponding results are therefore omitted. The study also reveals that this time for both wings, out of the six uncertain parameters, only one of them, namely the elastic axis position a has a major impact on gust loads. The corresponding metrics and sensitivity indices for the two distributions are reported in Tables C.10 and C.11.

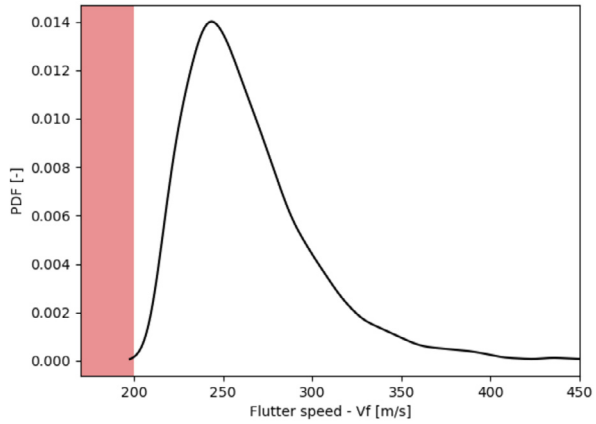

(a) Flutter speed distribution - baseline

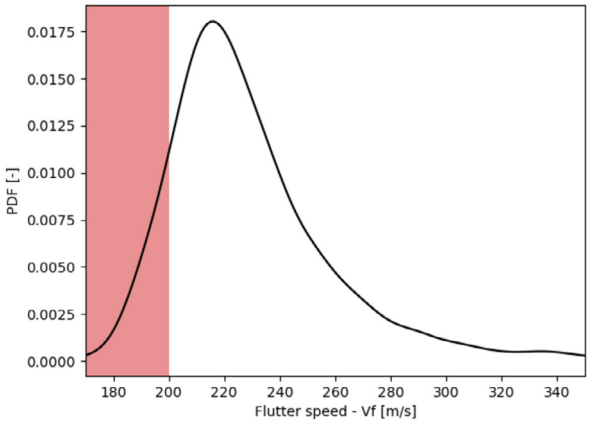

(b) Flutter speed distribution - 'stretched $\mathcal{AR}$ -15'

Fig. C.14. Flutter speed Probability Distribution Function following the uncertainty propagation on the baseline test-case. The area shed in red indicates the imposed flutter-safe region: the probability of flutter occurring within this region should be lower than 5%. The baseline results robust enough with respect to such condition.

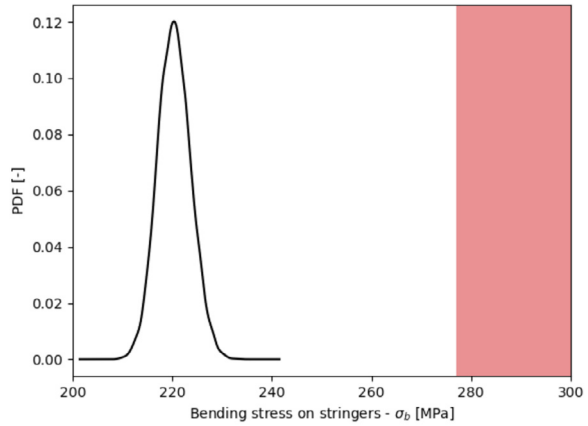

(a) Bending stress distribution - baseline

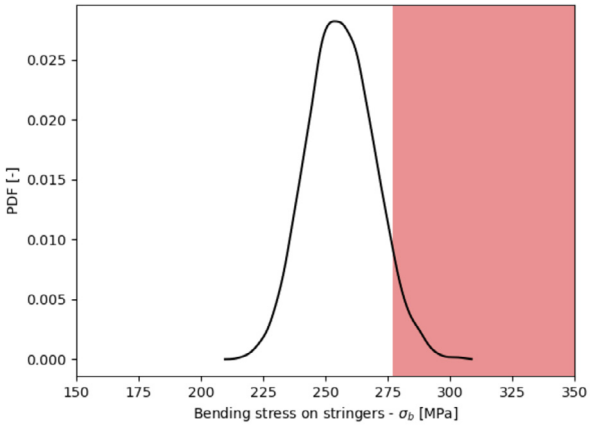

(b) Bending stress distribution - 'stretched $\mathcal{AR}$ -15'

Fig. C.15. Gust loads distributions following uncertainty propagation on the baseline (a) and 'stretched $\mathcal{AR}$ -15' (b) wings. The area shed in red indicates the imposed safe region: the probability of loads occurring within this region should be lower than 5%. The 'stretched $\mathcal{AR}$ -15' configuration does not result robust enough with respect to the bending loads.

Table C.11
Main statistical figures from the sensitivity analysis and uncertainty quantification on the gust-induced bending loads at wing root for the 'stretched $\mathcal{AR}$ -15' configuration. The highest Sobol indices, revealing the most impacting parameters, are highlighted in bold.

Distribution properties							
Mean	256 MPa						
Standard deviation	13 MPa						
95th percentile (P_{95})	279 MPa						
Sensitivity indices							
	a	d	μ	I	J	I_p	Sum
Sobol first	**0.98**	7.7e-4	1.4e-3	2.3e-3	0.01	4.2e-6	1.0
Sobol total	**0.98**	9.8e-4	1.4e-3	2.6e-3	0.01	1.8e-5	1.0

References

[1] N. Cumpsty, D. Mavris, M. Kirby, Aviation and the environment: outlook, ICAO environmental report 2019, Chapter 1, https://www.icao.int/environmentalprotection/Pages/environmentpublications.aspx, 2019.

[2] J. Green, et al., Air travel - greener by design mitigating the environmental impact of aviation: opportunities and priorities, Aeronaut. J. 109 (1099) (2005) 361–416, https://doi.org/10.1017/S0001924000000841.

[3] D. Maldonado, S.A. Viken, J.A. Housman, C.A. Hunter, J.C. Duensing, N.T. Frink, J.C. Jensen, S.N. McMillin, C.C. Kiris, Computational simulations of a Mach 0.745 transonic truss-braced wing design, in: AIAA Scitech 2020 Forum, 6-10 January 2020, Orlando, Florida, 2020.

[4] J. Vos, D. Charbonnier, T. Ludwig, S. Merazzi, H. Timmermans, D. Rajpal, A. Gehri, Aero-elastic simulations using the NSMB CFD solver including results for a Strut Braced Wing Aircraft, in: Flexible Engineering Toward Green Aircraft, in: Lecture Notes in Applied and Computational Mechanics, vol. 92, Springer, 2020, pp. 71–94.

[5] The Airbus Company, AlbatrossONE - a revolutionary approach to aircraft wing design, Airbus innovation portal, https://www.airbus.com/en/innovation/disruptive-concepts/biomimicry/albatrossone, 2019.

[6] F. Bocola, V. Muscarello, G. Quaranta, P. Masarati, Pilot in the loop aeroservoelastic simulation in support to the conceptual design of a fly by wire airplane, AIAA paper 2015-2557, in: AIAA Atmospheric Flight Mechanics Conference, 22-26 June, Dallas, TX, 2015, https://doi.org/10.2514/6.2015-2557.

[7] V. Trifari, M. Ruocco, V. Cusati, F. Nicolosi, A. De Marco, Multi-disciplinary analysis and optimization JAVA tool for aircraft design, in: 31st ICAS Congress, Belo Horizonte, Brazil, September 9–14, 2018, 2018.

[8] W. Su, C.E. Cesnik, Nonlinear aeroelasticity of a very flexible blended-wing-body aircraft, J. Aircr. 47 (5) (2010) 1539–1553.

[9] L. Cavagna, S. Ricci, L. Riccobene, A fast tool for structural sizing, aeroelastic analysis and optimization in aircraft conceptual design, AIAA paper 2009-2571 in: 50th AIAA/ASME/ASCE/AHS/ASC Structures, Structural Dynamics and Materials Conference, 4-7 May, Palm Springs, California, 2009.

[10] M. Drela, Tasopt 2.00, Tech. rep., Massachusetts Institute of Technology, 2010.

[11] L. Cavagna, S. Ricci, L. Travaglini, Aeroelastic analysis and optimization at conceptual design level using neocass suite, in: 52nd AIAA/ASME/ASCE/AHS/ASC Structures, Structural Dynamics and Materials Conference 19th AIAA/ASME/AHS Adaptive Structures Conference 13t, 2011, p. 2079.
[12] M.M. Opgenoord, M. Drela, K.E. Willcox, Influence of transonic flutter on the conceptual design of next-generation transport aircraft, AIAA J. 57 (5) (2019) 1973–1987.
[13] D. Colas, N.H. Roberts, V.S. Suryakumar, Hale multidisciplinary design optimization part I: solar-powered single and multiple-boom aircraft, in: 2018 Aviation Technology, Integration, and Operations Conference, 2018, p. 3028.
[14] D. Colas, N.H. Roberts, V.S. Suryakumar, Hale multidisciplinary design optimization part II: solar-powered flying-wing aircraft, in: 2018 Aviation Technology, Integration, and Operations Conference, 2018, p. 3029.
[15] A.B. Lambe, J. Martins, A unified description of MDO architectures, in: 9th World Congress on Structural and Multidisciplinary Optimization, Shizuoka, Japan, 2011.
[16] T.W. Simpson, J.R. Martins, Multidisciplinary design optimization for complex engineered systems: report from a national science foundation workshop, J. Mech. Des. 133 (10) (2011).
[17] J.S. Gray, J.T. Hwang, J.R.R.A. Martins, K.T. Moore, B.A. Naylor, OenMDAO: an open-source framework for multidisciplinary design, analysis, and optimization, Struct. Multidiscip. Optim. 59 (2019) 1075–1104, https://doi.org/10.1007/s00158-019-02211-z.
[18] M.J. Sasena, P. Papalambros, P. Goovaerts, Exploration of metamodeling sampling criteria for constrained global optimization, Eng. Optim. 34 (3) (2002) 263–278.
[19] N. Bartoli, T. Lefebvre, S. Dubreuil, R. Olivanti, R. Priem, N. Bons, J. Martins, J. Morlier, Adaptive modeling strategy for constrained global optimization with application to aerodynamic wing design, Aerosp. Sci. Technol. 90 (2019) 85–102, https://doi.org/10.1016/j.ast.2019.03.041.
[20] R. Priem, N. Bartoli, Y. Diouane, A. Sgueglia, Upper trust bound feasibility criterion for mixed constrained Bayesian optimization with application to aircraft design, Aerosp. Sci. Technol. 105 (2020) 105980.
[21] R. Priem, H. Gagnon, I. Chittick, S. Dufresne, Y. Diouane, N. Bartoli, An efficient application of Bayesian optimization to an industrial MDO framework for aircraft design, in: AIAA AVIATION 2020 FORUM, 2020, p. 3152.
[22] L. Wang, C. Xiong, J. Hu, X. Wang, Z. Qiu, Sequential multidisciplinary design optimization and reliability analysis under interval uncertainty, Aerosp. Sci. Technol. (2018), https://doi.org/10.1016/j.ast.2018.07.029.
[23] D.N. Mavris, O. Bandte, D.A. DeLaurentis, Robust design simulation: a probabilistic approach to multidisciplinary design, J. Aircr. 36 (1) (1999) 298–307.
[24] D.L. Clark, D.L. Allison, H. Bae, E.E. Forster, Effectiveness-based design of an aircraft considering mission uncertainties, J. Aircr. 56 (5) (2019) 1961–1972, https://doi.org/10.2514/1.C035402.
[25] J.M. Mines, A bi-level framework for aircraft design uncertainty quantification and management, Phd thesis, Georgia Institute of Technology, 2019.
[26] P. Schmollgruber, Enhancement of the conceptual aircraft design process through certification constraints management and full mission simulations, Phd thesis, Doctorat de l'Université de Toulouse délivré par l'Institut Supérieur de l'Aéronautique et de l'Espace (ISAE), Dec. 2018, https://hal.archives-ouvertes.fr/tel-02146110.
[27] A. Da Ronch, N.D. Tantaroudas, K.J. Badcock, J. Mottershead, A nonlinear controller for flutter suppression: from simulation to wind tunnel testing, AIAA paper 2014-0345, in: 55th AIAA/ASME/ASCE/AHS/ASC Structures, Structural Dynamics, and Materials Conference, 2014, pp. 1–19, https://doi.org/10.2514/6.2014-0345.
[28] Q. Zhou, D. Li, A. Da Ronch, G. Chen, Y. Li, Computational fluid dynamics-based transonic flutter suppression with control delay, J. Fluids Struct. 66 (2016) 183–206, https://doi.org/10.1016/j.jfluidstructs.2016.07.002.
[29] Y. Wang, F. Li, A. Da Ronch, Adaptive feedforward control design for gust loads alleviation of highly flexible aircraft, in: Proceedings of AIAA Atmospheric Flight Mechanics Conference, Dallas, Texas, 2015, 2015.
[30] M. Saporito, A. Da Ronch, Aeroelastic energy harvesting from statistically representative gust encounters, J. Fluids Struct. 94 (2020) 102869, https://doi.org/10.1016/j.jfluidstructs.2020.102869.
[31] Y. Wang, A. Da Ronch, M. Ghandchi-Tehrani, Adaptive feedforward control for gust-induced aeroelastic vibrations, Aerospace 3 (86) (2018), www.mdpi.com/journal/aerospace.
[32] Y. Fung, Fundamentals of flutter analysis, An Introduction to the Theory of Aeroelasticity, 1993, pp. 186–245.
[33] J.R. Wright, J.E. Cooper, Introduction to Aircraft Aeroelasticity and Loads, vol. 20, John Wiley & Sons, 2008.
[34] M.J. Patil, D.H. Hodges, On the importance of aerodynamic and structural geometrical nonlinearities in aeroelastic behavior of high-aspect-ratio wings, J. Fluids Struct. 19 (7) (2004) 905–915.
[35] D. Tang, E.H. Dowell, Experimental and theoretical study on aeroelastic response of high-aspect-ratio wings, AIAA J. 39 (8) (2001) 1430–1441.
[36] T. Theodorsen, General theory of aerodynamic instability and the mechanism of flutter, NACA Report No. 496, 1935, p. 24, arXiv:1011.1669v3.
[37] D. Calderon, J. Cooper, M. Lowenberg, S. Neild, E. Coetzee, Sizing high-aspect-ratio wings with a geometrically nonlinear beam model, J. Aircr. 56 (4) (2019) 1455–1470.
[38] W. Yu, Q. Wang, Geometrically exact beam theory, in: Composites Design and Manufacturing HUB, July 2014, https://cdmhub.org/resources/gebt.
[39] W. Yu, M. Blair, GEBT: a general-purpose nonlinear analysis tool for composite beams, Compos. Struct. 94 (2012) 2677–2689.
[40] Q. Wang, M.A. Yu, W. Sprague, J. Jonkman, Geometric nonlinear analysis of composite beams using Wiener-Milenkovic parameters, in: Proceedings of the 54th Structures, Structural Dynamics, and Materials Conference, 8-11 April 2013, Boston, Massachusetts, USA, 2013.
[41] H. Hesse, R. Palacios, Reduced-order aeroelastic models for dynamics of maneuvering flexible aircraft, AIAA J. 52 (8) (2014) 1717–1732, https://doi.org/10.2514/1.J052684.
[42] D. Kharlamov, Computational aeroelasticity for next-generation aircraft, Ph.D. thesis, University of Southampton, 2021.
[43] D.H. Hodges, X. Shang, C.E. Cesnik, Finite element solution of nonlinear intrinsic equations for curved composite beams, J. Am. Helicopter Soc. 41 (4) (1996) 313–321.
[44] M. Saporito, A. da Ronch, P. Schmollgruber, N. Bartoli, Framework development for robust design of novel aircraft concept, in: 3AF Aerospace Europe Conference, Feb 2020, BOR-DEAUX, France, 2020, hal-02904365.
[45] M. Saporito, A. Da Ronch, N. Bartoli, S. Defoort, Flying qualities reliability constraints in aircraft conceptual design using time-marching simulations, AIAA paper 2021-3101, in: AIAA AVIATION 2021 FORUM, August 2-6, 2021, Virtual Event, 2021, p. 3101.
[46] G. Quaranta, P. Masarati, P. Mantegazza, A conservative mesh-free approach for fluid-structure interface problems, in: International Conference on Computational Methods for Coupled Problems in Science and Engineering, Santorini, Greece, May 25-28, 2005, 2005.
[47] J.D. Anderson, Fundamentals of Aerodynamics, 5th edition, McGraw-Hill, 2011.
[48] R.L. Bisplinghoff, H. Ashley, R. Halfman, Aeroelasticity, Dover Publications, Inc., 1955.
[49] A. Sgueglia, Methodology for sizing and optimising a Blended Wing-Body with distributed electric ducted fans, Phd thesis, ISAE - Institut Supérieur de l'Aéronautique et de l'Espace, Dec. 2019, https://hal.archives-ouvertes.fr/tel-02487044.
[50] C. David, S. Delbecq, S. Defoort, P. Schmollgruber, E. Benard, V. Pommier-Budinger, From FAST to FAST-OAD: an open source framework for rapid overall aircraft design, IOP Conf. Ser., Mater. Sci. Eng. 1024 (1) (2021) 012062, https://doi.org/10.1088/1757-899x/1024/1/012062.
[51] E. Roux, Pour un approche analytique de la dinamique du vol, PhD Thesis, ISAE-SUPAERO, Toulouse, 2005.
[52] C.C. Dupont, W. P., Preliminary design of commercial transport aircraft, in: Didactic Material, ISAESupaero, Toulouse, France, 2012.
[53] V. Palladino, N. Bartoli, S. Dubreuil, E. Bénard, V. Pommier-Budinger, A. Jordan, P. Schmollgruber, S. Defoort, A comparative study of different propulsion models for hybrid electric aircraft, in: 3AF Aerospace Europe Conference 2020, Bordeaux, France, Feb. 2020, arXiv:https://hal.archives-ouvertes.fr/hal-02904367/file/DTIS20114.1590406781.pdf, https://hal.archives-ouvertes.fr/hal-02904367.
[54] A. Sgueglia, P. Schmollgruber, N. Bartoli, O. Atinault, E. Bénard, J. Morlier, Exploration and sizing of a large passenger aircraft with distributed electric ducted fans, AIAA paper 2018-1745, in: AIAA Scitech Forum, 8-12 January 2018, Kissimmee, US, 2018, pp. 1–33, arXiv:https://oatao.univ-toulouse.fr/19580/.
[55] A. Sgueglia, P. Schmollgruber, E. Bénard, N. Bartoli, J. Morlier, Preliminary sizing of a medium range blended wing-body using a multidisciplinary design analysis approach, MATEC Web Conf. 233 (2018) 1–9, https://doi.org/10.1051/matecconf/201823300014, arXiv:https://oatao.univ-toulouse.fr/21202/.
[56] A.G. Watson, R.J. Barnes, Infill sampling criteria to locate extremes, Math. Geol. 27 (5) (1995) 589–608.
[57] T. S., H. G., E.G. T., Uncertainpy: a python toolbox for uncertainty quantification and sensitivity analysis in computational neuroscience, Front. Neuroinform. (2018) 12–49, https://doi.org/10.3389/fninf.2018.00049.
[58] B. Sudret, Global sensitivity analysis using polynomial chaos expansions, Reliab. Eng. Syst. Saf. 93 (7) (2008) 964–979.
[59] C. Conlan-Smith, C. Schousboe Andreasen, Aeroelastic optimization of aircraft wings using a coupled three-dimensional panel-beam model, AIAA J. 59 (4) (2021) 1374–1386.
[60] S. Gudmundsson, General Aviation Aircraft Design: Applied Methods and Procedures, Butterworth-Heinemann, 2013.
[61] E. Panettieri, M. Montemurro, D. Fanteria, F. Coccia, Multi-scale least-weight design of a wing-box through a global/local modelling approach, J. Optim. Theory Appl. 187 (3) (2020) 776–799.
[62] European Aviation Safety Agency, Certification specifications and acceptable means of compliance for large aeroplanes - "aeroelastic stability requirements", CS-25, 25.629, Amendment 27, Dec 2021.

[63] US Federal Aviation Administration, Administration, Airworthiness standards: Transport category airplanes - “aeroelastic stability requirements”, CFR-25.629, 2021.
[64] European Aviation Safety Agency, Certification specifications and acceptable means of compliance for large aeroplanes - “gust and turbulence loads”, CS-25, 25.341, Amendment 27, Dec 2021.
[65] US Federal Aviation Administration, Administration, Airworthiness standards: Transport category airplanes - “gust and turbulence loads”, CFR-25.341, 2021.
[66] U.S. Federal Aviation Administration, Advisory Circular No 25.341-1 - Dynamic Gust Loads, 2014.